

Active Learning on a Budget: Opposite Strategies Suit High and Low Budgets

Guy Hacohen^{1,2} Avihu Dekel¹ Daphna Weinshall¹

Abstract

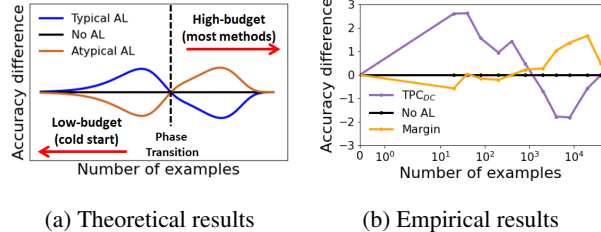
Investigating active learning, we focus on the relation between the number of labeled examples (budget size), and suitable corresponding querying strategies. Our theoretical analysis shows a behavior reminiscent of phase transition: typical points should best be queried in the low budget regime, while atypical (or uncertain) points are best queried when the budget is large. Combined evidence from our theoretical and empirical studies shows that a similar phenomenon occurs in simple classification models. Accordingly, we propose *TypiClust* – a deep active learning strategy suited for low budgets. In a comparative empirical investigation using a variety of architectures and image datasets, we report that in the low budget regime, *TypiClust* outperforms all other active learning strategies. Using *TypiClust* in a semi-supervised framework, the performance of competitive semi-supervised methods gets a significant boost, surpassing the state of the art.

1. Introduction

In recent years, with the advances in computational power and data accumulation, deep learning methods thrived, achieving the state of art in many benchmarks. However, these methods usually demand a large number of human-annotated data. While in many cases unlabeled data is relatively easy to achieve, human annotation remains costly.

Active Learning (AL) aims to alleviate this problem (see surveys in [Settles, 2009](#); [Schröder & Niebler, 2020](#)). Given a large pool of unlabeled data, and possibly a small set of labeled examples, learning is done iteratively: the learner employs the labeled examples (if any), then queries an oracle by submitting examples to be annotated. This may be done

¹School of Computer Science and Engineering, The Hebrew University of Jerusalem, Jerusalem, Israel ²Edmond & Lily Safra Center for Brain Sciences, The Hebrew University of Jerusalem, Jerusalem, Israel. Correspondence to: Guy Hacohen <guy.hacohen@mail.huji.ac.il>, Avihu Dekel <avihu.dekel@mail.huji.ac.il>, Daphna Weinshall <daphna@cs.huji.ac.il>.



(a) Theoretical results (b) Empirical results

Figure 1. Visualization of phase transition in deep active learning, as revealed by plotting the difference in accuracy between different AL strategies to a random baseline as a function of budget size (the number of queried examples). We see a similar behavior both theoretically and empirically: when the budget is low, oversampling typical examples is more beneficial, whereas when the budget is high, oversampling atypical examples is more beneficial. (a) The behavior of an idealized model (see Section 2). (b) The behavior of *TypiClust*, contrasted with a basic uncertainty-based strategy, as seen in deep neural models trained on CIFAR-10 (see Section 4).

repeatedly, often until a fixed budget is exhausted.

When submitting a query for a new label, two main principles guide the traditional active learning approach: (1) uncertainty sampling (e.g., [Lewis & Gale, 1994](#); [Scheffer et al., 2001](#); [Culotta & McCallum, 2005](#); [Joshi et al., 2009](#); [Li & Guo, 2013](#); [Ranganathan et al., 2017](#); [Gal et al., 2017](#); [Beluch et al., 2018](#); [Gissin & Shalev-Shwartz, 2019](#); [Yoo & Kweon, 2019](#); [Sinha et al., 2019](#)), and (2) diversity sampling (e.g., [Elhamifar et al., 2013](#); [Yang et al., 2015](#); [Wang et al., 2016](#); [Yin et al., 2017](#); [Zhdanov, 2019](#); [He et al., 2019](#); [Kirsch et al., 2019](#); [Ash et al., 2020](#); [Shui et al., 2020](#)). In uncertainty sampling, the learner queries examples about which it is least certain, presumably because such labels contain the most information about the problem at hand. In diversity sampling, queries are chosen to minimize the correlation between samples, to avoid redundancy in the annotations. Notably, as deep active learning is practical only in batch settings, the importance of diversity is amplified ([Geifman & El-Yaniv, 2017](#); [Sener & Savarese, 2018](#)).

At present, effective deep active learning strategies are known to require a large initial set of labeled examples to work properly ([Yuan et al., 2020](#); [Pourahmadi et al., 2021](#)). We call this the *high budget regime*, while the regime characterized by failure (or "cold start") is called the *low budget regime*. In the low budget regime, it has been shown that random selection outperforms most querying strategies (see

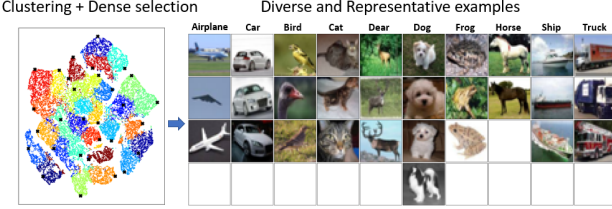


Figure 2. Visualizing the selection of 30 examples from CIFAR-10 by *TypiClust*. Left: the data is first clustered into 30 clusters, and the densest example within every cluster is queried. We show t-SNE dimensionality reduction of the feature space, colored by cluster assignment, where selected examples are marked by \times . Right: the selected images, organized column-wise by class. Note that the ensuing labeled set is approximately class-balanced, even though the queries are chosen without access to class labels.

Attenberg & Provost, 2010; Mittal et al., 2019; Zhu et al., 2019; Siméoni et al., 2021; Chandra et al., 2021). Different accounts have been offered to explain this observation: (i) failure to model uncertainty, which is more severe with a small budget of labels (Nguyen et al., 2015; Gal & Ghahramani, 2016); (ii) difficulty to accomplish diversity in high dimensional input spaces, where traditional metrics (such as the Euclidean distance) are not meaningful. In Section 4.3, we show that these accounts cannot fully explain the failure of uncertainty sampling in the low budget regime.

As a result, most deep active learning research is focused on the high-budget regime. Strategies designed to address the low-budget regime usually employ self-supervised or semi-supervised methods using the unlabeled pool (Gao et al., 2020; Hong et al., 2020; Mahmood et al., 2021). In the ensuing embedding, the estimation of uncertainty is often more reliable (Zhang et al., 2018).

In this paper, we start by showing a formal argument, which suggests that the uncertainty principle may be unsuited for the low-budget regime. We find that in the low-budget regime the most typical points should be queried, while points of high uncertainty should be deferred to higher budgets. More specifically, we analyze a mixture of two independent learners model. We then prove, under some mild assumptions, that such models yield better performance if the distribution of the training data is allowed to be biased. The preferred distribution depends on the number of labeled examples – when limited to only a few labels, it is beneficial to sample additional *typical* examples (to be defined more precisely below), while with a large budget of labels, it is beneficial to sample more *atypical* examples. This is illustrated in Fig. 1a for an ideal model.

Guided by this theoretical analysis, we propose *TypiClust* – a novel strategy for active learning in the low-budget regime. *TypiClust* utilizes the unlabeled data to estimate the typicality of unlabeled examples. To this end, *TypiClust* employs self-supervised representation learning and then estimates

each point’s density in this representation. Diversity is obtained by clustering the dataset and picking the densest examples from each cluster (see Fig. 2).

We evaluate *TypiClust* in three AL frameworks: (i) A pool-based supervised framework, which repetitively queries labels and uses them to train a deep network model. (ii) A pool-based supervised framework, which leverages self-supervised pre-trained embeddings. (iii) An initial pool semi-supervised framework, which queries labels once and also uses the remaining unlabeled examples to train a deep network model. This body of work is summarized in Fig. 3, plotting the accuracy gain over the random baseline in the three AL frameworks.

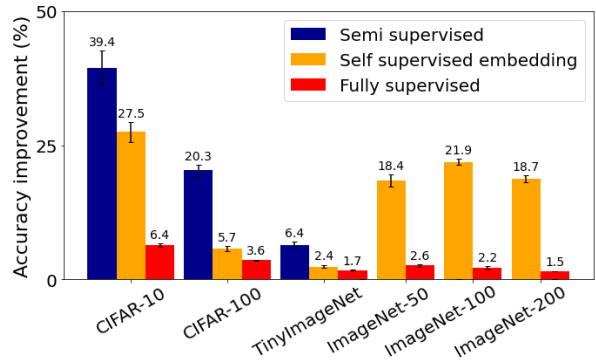


Figure 3. *TypiClust* achieves major accuracy gains as compared to the random selection baseline in the fully-supervised (3 repetitions on ImageNet, 10 otherwise), semi-supervised (3 reps) and self-supervised embedding (5 reps) frameworks. We use 10, 300, 1000, 50, 100, 200 examples in CIFAR-10, CIFAR-100, TinyImageNet, ImageNet-50, ImageNet-100 and ImageNet-200 respectively.

More specifically, our empirical study focuses on the low-budget regime. We first show that the aforementioned theoretical predictions are observed in practice when training competitive deep learning models on various image recognition benchmarks (see Fig. 1b). In accordance with Zhu et al. (2019), we also observe that many well-known querying strategies are not effective in this domain, and are even detrimental. In contrast, *TypiClust* consistently improves generalization by a large margin, across different datasets and architectures (see Fig. 3). We note that while the choice of a specific self-supervised task and a clustering algorithm may have an impact on performance, *TypiClust* remains beneficial (with significant gains) in all settings.

Although in both supervised and semi-supervised AL frameworks the learner has access to a big pool of unlabeled data, many AL strategies do not exploit the promise of semi-supervised learning. Recent studies report that the benefit of AL is marginal when semi-supervised learning methods are employed (Chan et al., 2021; Bengar et al., 2021), with little added value to the active querying of labels. Re-examining this observation, we note that semi-supervised learning is

most beneficial in the low-budget regime, wherein the explored AL strategies are inherently not suitable. By using *TypiClust*, which is designed for the low-budget regime, we show that AL outperforms random sampling in the semi-supervised framework by a large margin, surpassing the state-of-the-art (SOTA) performance on several image classification tasks.

Specifically, we used *TypiClust* to generate the labeled set for FlexMatch (Zhang et al., 2021), a competitive semi-supervised algorithm. With 10 queries from CIFAR-10, *TypiClust* improves the test accuracy of FlexMatch by 39.4% over a random selection. With 300 queries from CIFAR-100, *TypiClust* improves the accuracy of FlexMatch by 20.3%. This improvement is obtained even though *TypiClust* may not deliver a balanced training set, unlike the strategy against which it is compared.

1.1. Summary of Contribution

- We show theoretical and empirical results suggesting that typical examples are more important in low budgets, as opposed to atypical examples in high budgets.
- We propose a mixture learner model to analyze active learning; the model predicts a phase transition phenomenon that depends on the budget size.
- We empirically demonstrate this behavior in actual deep learning models trained on image benchmarks.
- We propose *TypiClust*: an AL strategy that significantly improves performance in the low budget regime.
- We empirically show that *TypiClust* can be used to boost SOTA semi-supervised learning methods.

2. Theoretical Analysis

We now introduce a simple mixture model of two learners, which reveals a phase-transition phenomenon in AL. Its relevance to actual classifiers is discussed in Section 2.3.

2.1. Mixture Model Definition

Active learning abandons random sampling in favor of biased sampling strategies. This can be formally investigated in the context of a mixture model. To this end, we start in Section 2.1.1 by defining such a mixture model. We then formalize biased data sampling strategies in Section 2.1.2.

2.1.1. MIXTURE LEARNER MODEL

We adopt a mixture of two learners model, where each learner is independently trained on a distinct part of the domain of the data distribution. Formally, let $\mathbf{X} = [\mathbf{x}, y]$ denote a single data point, where $\mathbf{x} \in \mathbb{R}^d$ denotes an input point and $y \in \mathbb{Y}$ its corresponding label or target value. For example, \mathbb{Y} is \mathbb{R} in regression problems, and $[k]$ in classification problems. Each point \mathbf{X} is drawn from a

distribution \mathcal{D} with density $f_{\mathcal{D}}(\mathbf{X})$. We denote an i.i.d sample of m points from \mathcal{D} as $\mathbb{X}^m = \{\mathbf{X}_1, \dots, \mathbf{X}_m\} \sim \mathcal{D}^m$.

Let $R_1, R_2 \subseteq \mathbb{R}^d \times \mathbb{Y}$ denote a partition of the domain of $f_{\mathcal{D}}$, where $R_1 \cup R_2 = \mathbb{R}^d \times \mathbb{Y}$ and $R_1 \cap R_2 = \emptyset$. Let $\mathcal{D}_1, \mathcal{D}_2$ denote the conditional distributions obtained when restricting \mathcal{D} to regions R_1, R_2 respectively. Note that \mathcal{D} can now be viewed as a mixture distribution, where points are sampled from \mathcal{D}_1 with probability $p = \int_{\mathbf{X} \in R_1} f_{\mathcal{D}}(\mathbf{X}) d\mathbf{X}$, and \mathcal{D}_2 with probability $(1 - p)$. Let $m_i, i \in \{1, 2\}$ denote the number of points in R_i when sampling m points from \mathcal{D} , and \mathbb{X}^{m_i} denote the restriction of sample \mathbb{X}^m to R_i . The hypothesis obtained when training a learner independently on \mathbb{X}^{m_i} is denoted $h(\mathbb{X}^{m_i})$.

Next, we define the error score of a learner, which is a function of m - the training set size. It measures the expected generalization error of the learner over all such training sets.

Definition 1 (Error score). *Assume training sample $\mathbb{X}^m \sim \mathcal{D}^m$, with the corresponding learned hypothesis $h(\mathbb{X}^m)$. Let $Er(\mathbf{X}, h(\mathbb{X}^m))$ denote the error of this hypothesis on some point $\mathbf{X} \in \mathbb{R}^d \times \mathbb{Y}$. The expected error of the learner, over random variables \mathbf{X} , \mathbb{X}^m and $h(\mathbb{X}^m)$, is given by*

$$E_{\mathcal{D}}(m) = \mathbb{E}_{\mathbf{X}} [\mathbb{E}_{\mathbb{X}^m} [\mathbb{E}_{h(\mathbb{X}^m)} [Er(\mathbf{X}, h(\mathbb{X}^m))]]] \quad (1)$$

We make two commonly adopted assumptions on $E_{\mathcal{D}}(m)$: (i) **Efficiency**. $E_{\mathcal{D}}(m)$ is strictly monotonically decreasing, namely, on average the learner benefits from additional examples. (ii) **Realizability**. $\lim_{m \rightarrow \infty} E_{\mathcal{D}}(m) = 0$.

During training, we assume a mixture of independent learners in R_1, R_2 , and a training set composed of m_1, m_2 examples from each region respectively. The error score of the mixture learner on \mathcal{D} for $m = m_2 + m_1$ is:

$$E_{\mathcal{D}}(m) = p \cdot E_{\mathcal{D}_1}(m_1) + (1 - p) \cdot E_{\mathcal{D}_2}(m_2) \quad (2)$$

As an important ingredient of the mixture model, we assume that one region requires fewer examples to be adequately learned, and call this region R_1 . Essentially, we expect the error score to decrease faster at R_1 , with $E_{\mathcal{D}_1}(m) < E_{\mathcal{D}_2}(m) \forall m$. Other than this difference, we expect the error score to be similar in R_1 and R_2 . Making all this more precise, we formally assume that the error scores in R_1, R_2 can be written as $E_{\mathcal{D}_1}(m) = E(m)$ and $E_{\mathcal{D}_2}(m) = E(\alpha m)$ for a single function $E(m)$ and learning speed parameter $\alpha \leq 1$. We can now rewrite (2) as follows:

$$E_{\mathcal{D}}(m) = p \cdot E(m_1) + (1 - p) \cdot E(\alpha(m - m_1)) \quad (3)$$

Finally, we extend $E(m)$ to domain \mathbb{R}^+ with the continuation of $E(m)$ denoted $E(x) : \mathbb{R}^+ \rightarrow \mathbb{R}^+$, which is in C^∞ and positive. **Efficiency** is extended to imply $E'(x) < 0$.

2.1.2. SAMPLING STRATEGIES

Considering the extended error score $E(x) : \mathbb{R}^+ \rightarrow \mathbb{R}^+$, we define a biased sampling strategy as follows:

$$m_1 = p \cdot m + \Delta, \quad m_2 = (1 - p) \cdot m - \Delta$$

$\Delta = 0$ is essentially equivalent to random sampling from \mathcal{D} . $\Delta > 0$ implies that more training points are sampled from R_1 than R_2 , and vice versa.

In Thm. 1 we show that when aiming to minimize the expected generalization error while considering a mixture of 2 learners model as defined above, choosing between the different sampling strategies can be done using a simple threshold test. The proof for Thm. 1 can be found in App B.1.

Theorem 1. *Let $0 < p < 1$, $0 < \alpha < \frac{p}{1-p}$ denote some constants. Given error score $E(x)$, the following threshold test decreases the expected error for sample size m :*

$$\frac{E'(pm)}{E'(\alpha(1-p)m)} \begin{cases} > \frac{\alpha(1-p)}{p} & \Rightarrow \text{over sample region } R_1 \\ < \frac{\alpha(1-p)}{p} & \Rightarrow \text{over sample region } R_2 \end{cases}$$

Example: exponentially decreasing function. Assume $E(m) = e^{-m}$, and a mixture model with $p = 0.8, \alpha = 0.1$. We simulate $E(m)$ when biasing the train sample with $\Delta = \pm 0.01$. Fig. 1a shows the differences between the error score of biased sampling (in favor of either R_1 in blue or R_2 in orange) and random sampling, as a function of the number of examples m . For small m it is beneficial to favorably bias region R_1 , while for large m it is beneficial to favorably bias R_2 . This is the behavior often seen in our empirical investigation, see Fig. 1b and Section 4.

2.2. Error Scores Analyzed

We now report sufficient conditions on $E(m)$, which guarantee the phase-transition-like behavior illustrated in Fig. 1a. We start with some formal definitions, and then obtain sufficient conditions for these definitions to take hold.

To capture the sought behavior, we say that an error score is undulating if it displays at least two phases. In the beginning, with only a few training examples, such learners benefit from over-sampling region R_1 . After seeing sufficiently many training examples, such learners may benefit from over-sampling region R_2 . Formally:

Definition 2 (Undulating). *An error score $E(m)$ is undulating if there exist $z_1, z_2 \in \mathbb{R}$ such that $\frac{E'(pm)}{E'(\alpha(1-p)m)} > \frac{\alpha(1-p)}{p} \quad \forall m < z_1$, and $\frac{E'(pm)}{E'(\alpha(1-p)m)} < \frac{\alpha(1-p)}{p} \quad \forall m > z_2$.*

For undulating error scores, there could potentially be any number of transitions between the two conditions, switching

the preference of R_1 to R_2 , and vice versa. We extend the above definition to capture a case of particular interest, where this transition happens only once, as follows:

Definition 3 (SP-undulating). *An error score $E(m)$ is Single-Phase undulating if it is undulating, and $z_1 = z_2$.*

2.2.1. UNDULATING ERROR SCORES

As motivated in Section 2.1.1, we define a proper error score as follows:

Definition 4 (Proper error score). *$E(x) : \mathbb{R}^+ \rightarrow \mathbb{R}^+$ is a proper error score if it is a positive twice differentiable function, which is strictly monotonically decreasing ($E > 0, E' < 0$), $E(0) = c_0 \in \mathbb{R}_*^+$, and where $\lim_{x \rightarrow \infty} E(x) = 0$.*

Not all proper error scores will exhibit the phase undulating behavior. In Thm. 2 we state sufficient conditions that ensure this behavior (see proof in App B.2).

Theorem 2 (Undulating error score: sufficient conditions). *Let $0 < p < 1, 0 < \alpha < \frac{p}{1-p}$ denote some constants. Error score $E(x)$ is undulating if the following assumptions hold:*

1. $E(x)$ is a proper error score (see Def. 4)
2. $\lim_{x \rightarrow \infty} \frac{E'(x)}{E(x)}, \lim_{x \rightarrow \infty} \frac{E(x)}{E(ax)}, \lim_{x \rightarrow \infty} \frac{E'(x)}{E'(ax)}$ exist $\forall a \in (0, 1)$
3. $-\log(E(x)) = \omega(\log(x))$

Corollary 1 (Exponential error as a bound). *Error score $E(x)$ is undulating if it satisfies assumptions (1) and (2) of Thm. 2, and is bounded from above as follows*

$$E(x) \leq ke^{-\nu x} \quad \forall x \in \mathbb{R}^+ \quad (4)$$

for some constants $\nu, k \in \mathbb{R}_*^+$.

Proof. It can be readily verified that assumption (3) of Thm. 2 follows from (4). \square

2.2.2. SP-UNDULATING ERROR SCORES

Thm. 3 extends the results of the previous section, by stating a set of sufficient conditions that ensure an SP-undulating error score. The proof can be found in App B.3.

Theorem 3 (SP-undulating: sufficient conditions). *Let $0 < p < 1, 0 < \alpha < \frac{p}{1-p}$ denote some constants. Error score $E(x)$ is SP-undulating if the following assumptions hold:*

1. $E(x)$ is an undulating proper error score.
2. At least one of the following conditions holds:
 - (a) $\frac{-E''(x) \cdot x}{E'(x)}$ is monotonically increasing with x .
 - (b) $-E'(x)$ is strictly monotonically decreasing and log-concave.

Corollary 2 (Exponential error is SP-undulating). *Consider error scores of the form $E(x) = ke^{-\nu x}$ for constants $\nu, k \in \mathbb{R}_*^+$. Such functions are SP-undulating.*

Cor. 2 shows that classifiers with an exponentially decreasing *error score* are SP-undulating, with a single transition from favoring R_1 to favoring R_2 .

In practice, we cannot assume that the *error score* of commonly used learners is exponentially decreasing. However, frequently we can bound the *error score* from above by an exponentially decreasing function, as we demonstrate theoretically (see Section 2.3.1) and empirically (see Fig. 14 in the App). In such cases, it follows from Cor. 1 that these functions are undulating.

2.3. Simple Classification Models

To make the analysis above more concrete, we analyze a mixture of two linear classifiers in Section 2.3.1. We then analyze the nearest neighbors classification model in Section 2.3.2, to shed light on the circumstances that make it possible to learn from fewer examples in certain regions.

2.3.1. MIXTURE OF TWO LINEAR CLASSIFIERS

Consider a binary classification problem and assume a learner that delivers a mixture of two linear classifiers in \mathbb{R}^d . The two classifiers are obtained by independently minimizing the L_2 loss on points in R_1 and R_2 respectively.

I. Bounding the error of each mixture component. We first derive a bound on the error of the j^{th} component, as it depends on the sample size m_j . Let $X \in \mathbb{R}^{d \times m_j}$ denote the matrix whose columns are the training vectors that lie in region R_j . Let $\mathbf{y} \in \{-1, 1\}^{m_j}$ denote a row labels vector, where 1 marks positive examples and -1 negative examples. The learner seeks a separating row vector $\hat{\mathbf{w}} \in \mathbb{R}^d$, where

$$\hat{\mathbf{w}} = \arg \min_{\mathbf{w} \in \mathbb{R}^d} \|\mathbf{w}X - \mathbf{y}\|^2 \implies \hat{\mathbf{w}} = \mathbf{y}X^\top(XX^\top)^{-1}$$

In Thm. 4, we bound the error of a linear model by some exponential function of the number of training examples m_j . The proof and further details can be found in App C.1.

Theorem 4 (Error bound on a linear classifier). *Assume: (i) a bounded sample $\|\mathbf{x}_i\| \leq B$, where X is sufficiently far from singular so that its smallest positive singular value is bounded from below by $\frac{1}{\Lambda}$; (ii) a realizable binary problem where the classes are separable by margin δ ; (iii) full rank data covariance, where $\frac{1}{\Lambda}$ denotes its smallest singular value. Then there exist some positive constants $k, \nu > 0$, such that $\forall m_j \in \mathbb{N}$ and every sample \mathbb{X}^{m_j} , the expected error of $\hat{\mathbf{w}}$ obtained using \mathbb{X}^{m_j} is bounded by:*

$$\mathbb{E}_{\mathbf{X} \sim \mathcal{D}_j} [0 - 1 \text{ loss of } \hat{\mathbf{w}}] \leq ke^{-\nu m_j} \quad (5)$$

II. A mixture classifier. Assume a mixture of two linear classifiers, and let $E(m) = p \cdot E_{\mathcal{D}_1}(m_1) + (1-p) \cdot E_{\mathcal{D}_2}(m_2)$ denote its error score. The following theorem characterizes this function (the proof can be found in App C.1):

Theorem 5 (Undulating error). *Retain the assumptions stated in Thm. 4, and assume in addition that $\forall a \in (0, 1)$ $\exists \lim_{m \rightarrow \infty} \frac{E'(m)}{E(m)}, \lim_{m \rightarrow \infty} \frac{E(m)}{E(am)}, \lim_{m \rightarrow \infty} \frac{E'(m)}{E'(am)}$. Then the error score of a mixture of two linear classifiers is undulating.*

In practice, the *error score* in this case is also SP-undulating. The empirical validation of this point can be seen in Fig. 13.

2.3.2. KNN CLASSIFIER AND HIGH-DENSITY REGIONS

Our analysis in Section 2.2 showed that given some partition of the data into R_1 and R_2 , where R_1 is easier to learn in the sense that $E_{\mathcal{D}_{R_2}}(m) < E_{\mathcal{D}_{R_1}}(m)$ for every m , then oversampling from R_1 is preferable in the low budget regime, while oversampling from R_2 is preferable in the high budget regime. We now employ the discrete one-Nearest-Neighbor (1-NN) classification framework to shed light on the nature of the assumed partition. Specifically, we show that **selecting R_1 as the set of the densest points in the dataset** has the desired property. In fact, we show in App C.2 that in this framework, the selection of an initial pool of size m will benefit from the following heuristic:

- **Max density:** when selecting a point \mathbf{X}_i , maximize its density $f_{\mathcal{D}}(\mathbf{X}_i)$.
- **Diversity:** select points that are far apart, so that their corresponding sets of nearest neighbors do not overlap.

While 1-NN is a rather simplistic model, we propose to use the derived heuristics to guide deep active learning. In the rest of this paper, we show how these guiding principles benefit deep active learning in the low-budget regime.

3. Method: Low Budget Active Learning

In the low-budget regime, our theoretical analysis showed that it may be beneficial to bias the training sample in favor of certain regions in the data domain. It also established a connection between such regions and the principles of *max density* (or *typicality*) and *diversity*. In this section, we incorporate these principles into a new active learning strategy called *TypiClust*, designed for the low-budget regime.

3.1. Framework and Definitions

Let L_0 denote an initial labeled set of examples, and U_0 denote an initial unlabeled pool. Active learning is done iteratively: at each iteration i , a set of size B of unlabeled examples is picked according to some strategy. These examples are annotated by an oracle, added to L_i , and removed from U_i . This process is repeated until the label budget is exhausted, or some predefined termination conditions are satisfied. In the low-budget regime, the total number of labeled examples, represented by L_0 and B , is small. The case where $L_0 = \emptyset$ is called "initial pool selection".

3.2. Proposed Strategy: Typical Clustering (*TypiClust*)

We define the *Typicality* of an example by its density in some semantically meaningful feature space. Formally, we measure an example's *Typicality* by the inverse of the average Euclidean distance to its K nearest neighbors¹, namely:

$$\text{Typicality}(x) = \left(\frac{1}{K} \sum_{x_i \in \text{K-NN}(x)} \|x - x_i\|_2 \right)^{-1} \quad (6)$$

In the low budget regime, an active learning strategy based on typical examples needs to overcome several obstacles: (a) Networks trained on only a few examples are prone to overfit, making measures of typicality noisy and unreliable. (b) Typical examples tend to be very similar, amplifying the need for diversity (see App A.1 for further details).

To overcome these obstacles we propose a novel method, called *TypiClust*, which attempts to select typical examples while probing different regions of the data distribution. In our method, self-supervised representation learning is used to overcome (a), while clustering is used to overcome (b). *TypiClust* is therefore composed of 3 steps:

Step 1: Representation learning. Utilize the large unlabeled pool U_0 to learn a semantically meaningful feature space: first train a deep self-supervised task on $U_0 \cup L_0$, then use the penultimate layer of the resulting model as feature space. Such methods are commonly used for semantic feature extraction (Chen et al., 2020; Grill et al., 2020).

Step 2: Clustering for diversity. As *typicality* in (6) is evaluated by measuring distances to neighboring points, the most typical examples are usually close to each other, often resembling the same image (see Fig. 9c). To enforce diversity and thus better represent the underlying data distribution, we employ clustering. Specifically, at each AL iteration i , we partition the data into $|L_{i-1}| + B$ clusters. This choice guarantees that there are at least B clusters that do not intersect with the existing labeled examples. We refer to such clusters as *uncovered clusters*. All the implementation details can be found in App E.2.

Step 3: Querying typical examples. We select the most typical examples from the B largest *uncovered clusters*. Selecting from *uncovered clusters* enforces diversity (also w.r.t L_{i-1}), while selecting the most typical example in every cluster favors the selection of representative examples.

As the general steps above do not depend on the specific representation or clustering algorithm, different variants of the *TypiClust* strategy can be constructed for different tasks. In our work we consider two variants, both of which outperform by a large margin the uncertainty based strategies in the low-budget regime:

1. TPC_{DC} : Using a deep clustering algorithm both for the self-supervised and clustering tasks. In our experiments, we used SCAN (Van Gansbeke et al., 2020).
2. TPC_{RP} : Using representation learning followed by a clustering algorithm. We used DINO (Caron et al., 2021) for ImageNet, and SimCLR (Chen et al., 2020) for all other datasets, followed by K-means.

The pseudo-code of *TypiClust* can be found in Alg. 1 in App E.1. Note that, unlike traditional active learning strategies, *TypiClust* relies on self-supervised representation learning, and therefore can be used for initial pool selection.

4. Empirical Study

In this section we report a set of empirical results, demonstrating the benefits of *TypiClust* in the low-budget regime. Section 4.1 describes the evaluation protocol, specific datasets, and alternative methods. Section 4.2 describes the actual experiments and their results.

4.1. Methodology

We evaluate active learning separately in the following three frameworks. (i) **Fully supervised**: training a deep network solely on the labeled set, obtained by active queries. (ii) **Fully supervised using self-supervised embeddings**: training a linear classifier on the embedding obtained from a pre-trained self-supervised model. (iii) **Semi-supervised**: training a deep network on the labeled and unlabeled sets, using FlexMatch – a competitive semi-supervised algorithm.

In (i) and (ii), we adopted the AL evaluation framework created by Munjal et al. (2020), which implements several AL methods, including all baselines used here. In (iii) we adopted the code and hyper-parameters provided by FlexMatch. As FlexMatch is computationally intensive, we did not evaluate it on ImageNet, confining the study to datasets it has been reported to handle; in all of them, *TypiClust* is beneficial. For all implementation details, see App E.3.

We compared *TypiClust* to the following baseline strategies for the selection of B points from U : (1) *Random* – uniformly. (2) *Uncertainty* – lowest max softmax output. (3) *Margin* – lowest margin between the two highest softmax outputs. (4) *Entropy* – highest entropy of softmax outputs. (5) *DBAL* (Gal et al., 2017). (6) *CoreSet* (Sener & Savarese, 2018). (7) *BALD* (Kirsch et al., 2019). All strategies are evaluated on several image classification tasks, including CIFAR-10/100 (Krizhevsky et al., 2009), TinyImageNet (Le & Yang, 2015) and ImageNet-50/100/200, which are subsets of ImageNet (Deng et al., 2009) containing 50/100/200 classes respectively (following Van Gansbeke et al., 2020). All code will be published upon acceptance.

¹We use $K = 20$, but other choices yield similar results.

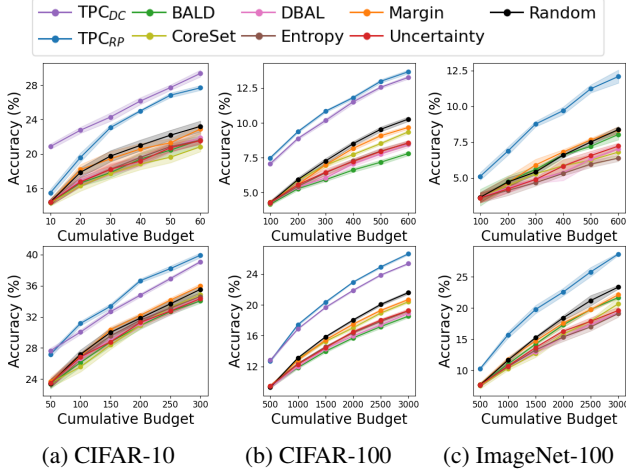


Figure 4. Framework (i): comparing *TypiClust* with baseline AL strategies on CIFAR-10, CIFAR-100, and ImageNet-100 for 5 active learning iterations in the low budget regime. The budget B is equal to (top) the number of classes, or (bottom) 5 times the number of classes. The final averaged test accuracy in each iteration is reported, using 10 (CIFAR) and 3 (ImageNet) repetitions. The shaded area reflects the standard error across repetitions.

4.2. Results: Low Budget Regime

The amount of labeled data that should be considered as low-budget is likely to vary between tasks. In the following experiments, unlike many previous works, we focus on scenarios where $0.02\% \sim 12\%$ of the examples are labeled.

(i) Fully supervised framework. Fig. 4 shows the accuracy of networks trained on CIFAR-10, CIFAR-100, and ImageNet-100, using the labeled examples queried by the different AL strategies. Denoting the number of classes by M , we use a budget of either $B = M$ or $B = 5M$ labeled examples, with $L_0 = \emptyset$. See App F.1 for other budget sizes.

We see that in the low budget regime, both *TypiClust* variants outperform the baselines by a large margin. Specifically, all other baseline AL methods perform on par with random selection or worse, in accordance with Pourahmadi et al. (2021). In contrast, the typicality-based strategy achieves a large gain in accuracy. Noting that most of the baselines are possibly hampered by their use of random initial pool selection when $L_0 = \emptyset$, our ablation study in Section 4.3.1 demonstrates that this is not the decisive factor.

(ii) Fully supervised with self-supervised embedding. As self-supervised embeddings can be semantically meaningful, they are often used as features for a linear classifier. Accordingly, in this framework, we use the extracted features from the representation learning step and train a linear classifier on the queried labeled set L_i . Unlike the fully supervised framework, here we use the unlabeled data while training the classifier, albeit in a basic manner. This framework outperforms the fully supervised framework, but still

lags behind the semi-supervised framework. Once again, *TypiClust* outperforms all baselines by a large margin, as shown in Fig. 5 (see App F.2 for additional datasets).

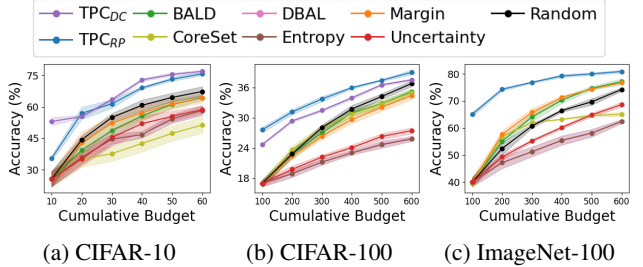


Figure 5. Similar to Fig. 4 in framework (ii), where a linear classifier is trained on features from a pre-trained self-supervised model.

(iii) Semi-supervised framework. In this framework, we evaluate *TypiClust* and different AL strategies by examining the performance of FlexMatch when trained on their respective queried examples. As semi-supervised methods often achieve competitive performance with only a few labeled examples, we focus on the extreme low-budget regime, where only $0.02\% \sim 1\%$ of the data is labeled. Note that semi-supervised algorithms typically assume a class-balanced labeled set, which is not feasible in active learning. To compare with this scenario which dominates the literature, we add a balanced random baseline for reference.

In Fig. 6, we compare the final performance of FlexMatch using the labeled sets provided by different AL strategies. We show results for a budget of 10 examples in CIFAR-10 (Fig. 6a), 300 examples in CIFAR-100 (Fig. 6b), and 1000 examples in TinyImageNet (Fig. 6c). We see that both *TypiClust* variants outperform random sampling, whether balanced or not, by a large margin. In contrast, other AL baselines do not improve the results of random sampling. Similar results using additional budgets, baselines, datasets, and semi-supervised algorithms, can be found in App F.3.

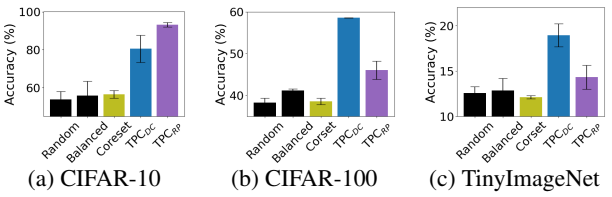


Figure 6. Comparison of AL strategies in a semi-supervised task. Each bar shows the mean test accuracy after 3 repetitions of FlexMatch trained on: (a) 10 examples from CIFAR-10, (b) 300 examples from CIFAR-100, (c) 1000 examples from TinyImageNet. Error bars denote the standard error.

4.3. Ablation Study

We now report the results of a set of ablation studies, checking the added value of each step in our suggested strategy.

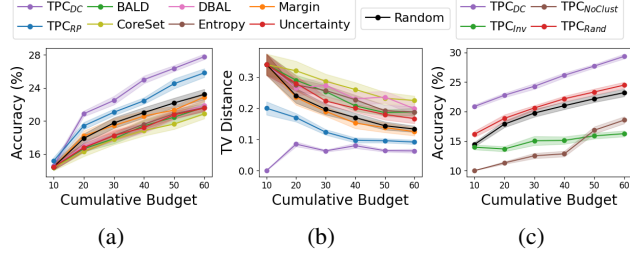


Figure 7. (a-b) Same experiment as in Fig. 4a top, but where: (a) *TypiClust* uses random initial set selection; (b) the Total Variation (TV) distance between the labeled set distribution and the ground truth class distribution is shown. (c) To isolate the added value of clustering for diversity and typical sample selection, we evaluate 3 additional selection heuristics on CIFAR-10 (see Section 4.3.3).

4.3.1. RANDOM INITIAL POOL SELECTION

As our AL strategies are based on self-supervised learning, they are well suited for the case $L_0 = \emptyset$, and can actively query the initial selection of labeled examples. By contrast, the other AL baselines use random initial pool selection when $L_0 = \emptyset$. To isolate the effect of this difference, we conducted the same experiment as reported in Fig. 4a, giving *TypiClust* a random initial pool selection just like the other baselines. Results are reported in Fig. 7a, showing that *TypiClust* still outperforms all baselines. Importantly, this comparison reveals that non-random initial pool selection yields further generalization gains when combined with active learning, which is useful in real-life problems.

4.3.2. COMPARING CLASS DISTRIBUTION

With an extremely low budget, covering the support of the distribution comprehensively is challenging. To compare the success of the different AL strategies in this task, we measure the Total Variation (TV) distance between the labeled set class distribution and the ground truth class distribution on each strategy. Fig. 7b shows that *TypiClust* variants achieve a significantly better (lower) score than the alternatives, resulting in queries with a better class balance.

4.3.3. THE IMPORTANCE OF DENSITY AND DIVERSITY

TypiClust clusters the dataset and selects the most typical examples from every cluster. To assess the added value of clustering and typicality selection, we consider the following alternative selection criteria: (a) Select a random example from each cluster (TPC_{Rand}). (b) Select the most atypical example in every cluster (TPC_{Inv}). (c) Select typical samples greedily, without clustering (TPC_{NoClust}).

The results in Fig. 7c show that both clustering and high-density sampling are crucial for the success of *TypiClust*. The low performance of TPC_{Rand} shows that representation learning and clustering alone cannot account for all the performance gain, while the low performance of TPC_{NoClust} shows that typicality without diversity is not sufficient.

4.3.4. UNCERTAINTY DELIVERED BY AN ORACLE

When trained on only a few labeled examples, neural networks tend to overfit, which may result in the unreliable estimation of uncertainty. This offers an alternative explanation to our results – uncertain examples may be a good choice in the low-budget regime as well, if only we could compute uncertainty accurately.

To test this hypothesis we first train an "oracle" network (see App. E.4) on the entire CIFAR-10 dataset and use its softmax margin to estimate uncertainty. This "oracle margin" is a more reliable uncertainty measure, which is then used to choose the query examples. Subsequently, another network is trained similarly to the setup of Fig. 4a, adding in each iteration the examples with either the highest or lowest softmax response margin according to the oracle.

The results are shown in Fig. 8. We see that even a reliable measure of uncertainty leads to poor performance in the low-budget regime, even worse than the baseline uncertainty-based methods. This may be because these methods compute the uncertainty in an unreliable way, and thus behave more like the random selection strategy.

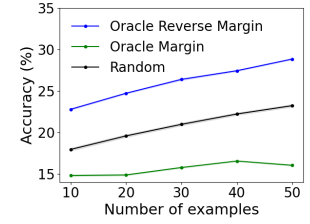


Figure 8. Certainty, as estimated by the margin of an oracle that knows the labels, is used for AL. We plot mean test accuracy of 100 models trained on CIFAR-10, $|L_0| = 10$, $B = 10$.

5. Summary and Discussion

We show, theoretically and empirically, that strategies for active learning in the high and low-budget regimes should be based on opposite principles. Initially, in the low budget regime, the most typical examples, which the learner can learn most easily, are the most helpful to the learner. When reaching the high-budget regime, the best examples to query are those that the learner finds most confusing. This is the case both in the fully supervised and semi-supervised settings: we show that semi-supervised algorithms get a significant boost from seeing the labels of typical examples.

Our results are closely related to curriculum learning (Bengio et al., 2009; Hacohen & Weinshall, 2019), hard data mining, and self-paced learning (Kumar et al., 2010), all of which reflect the added value of typical ('easy') examples when there is little information about the task, as against atypical ('hard') examples which are more beneficial later on. The point of transition - what makes the budget 'small' or 'large', depends on the task and corresponding data distribution. In complex real-life problems, the low budget regime may still contain a large number of examples, in-

creasing the usefulness of our method. Determining the range of training sizes with 'low budget' characteristics is a challenging problem, which we leave for future work.

References

Ash, J. T., Zhang, C., Krishnamurthy, A., Langford, J., and Agarwal, A. Deep batch active learning by diverse, uncertain gradient lower bounds. In *8th International Conference on Learning Representations, ICLR 2020, Addis Ababa, Ethiopia, April 26-30, 2020*. OpenReview.net, 2020.

Attenberg, J. and Provost, F. Why label when you can search? alternatives to active learning for applying human resources to build classification models under extreme class imbalance. In *Proceedings of the 16th ACM SIGKDD international conference on Knowledge discovery and data mining*, pp. 423–432, 2010.

Beluch, W. H., Genewein, T., Nürnberger, A., and Köhler, J. M. The power of ensembles for active learning in image classification. In *Proceedings of the IEEE Conference on Computer Vision and Pattern Recognition*, pp. 9368–9377, 2018.

Bengar, J. Z., van de Weijer, J., Twardowski, B., and Raducanu, B. Reducing label effort: Self-supervised meets active learning. In *Proceedings of the IEEE/CVF International Conference on Computer Vision*, pp. 1631–1639, 2021.

Bengio, Y., Louradour, J., Collobert, R., and Weston, J. Curriculum learning. In *Proceedings of the 26th annual international conference on machine learning*, pp. 41–48, 2009.

Caron, M., Touvron, H., Misra, I., Jégou, H., Mairal, J., Bojanowski, P., and Joulin, A. Emerging properties in self-supervised vision transformers. *arXiv preprint arXiv:2104.14294*, 2021.

Chan, Y.-C., Li, M., and Oymak, S. On the marginal benefit of active learning: Does self-supervision eat its cake? In *ICASSP 2021-2021 IEEE International Conference on Acoustics, Speech and Signal Processing (ICASSP)*, pp. 3455–3459. IEEE, 2021.

Chandra, A. L., Desai, S. V., Devaguptapu, C., and Balasubramanian, V. N. On initial pools for deep active learning. In *NeurIPS 2020 Workshop on Pre-registration in Machine Learning*, pp. 14–32. PMLR, 2021.

Chen, T., Kornblith, S., Norouzi, M., and Hinton, G. A simple framework for contrastive learning of visual representations. In *International conference on machine learning*, pp. 1597–1607. PMLR, 2020.

Cubuk, E. D., Zoph, B., Shlens, J., and Le, Q. V. Randaugment: Practical automated data augmentation with a reduced search space. In *Proceedings of the IEEE/CVF Conference on Computer Vision and Pattern Recognition Workshops*, pp. 702–703, 2020.

Culotta, A. and McCallum, A. Reducing labeling effort for structured prediction tasks. In *AAAI*, volume 5, pp. 746–751, 2005.

Deng, J., Dong, W., Socher, R., Li, L.-J., Li, K., and Fei-Fei, L. Imagenet: A large-scale hierarchical image database. In *2009 IEEE conference on computer vision and pattern recognition*, pp. 248–255. Ieee, 2009.

Elhamifar, E., Sapiro, G., Yang, A., and Sarsly, S. S. A convex optimization framework for active learning. In *Proceedings of the IEEE International Conference on Computer Vision*, pp. 209–216, 2013.

Gal, Y. and Ghahramani, Z. Dropout as a bayesian approximation: Representing model uncertainty in deep learning. In *international conference on machine learning*, pp. 1050–1059. PMLR, 2016.

Gal, Y., Islam, R., and Ghahramani, Z. Deep bayesian active learning with image data. In *International Conference on Machine Learning*, pp. 1183–1192. PMLR, 2017.

Gao, M., Zhang, Z., Yu, G., Arik, S. Ö., Davis, L. S., and Pfister, T. Consistency-based semi-supervised active learning: Towards minimizing labeling cost. In *European Conference on Computer Vision*, pp. 510–526. Springer, 2020.

Geifman, Y. and El-Yaniv, R. Deep active learning over the long tail. *arXiv preprint arXiv:1711.00941*, 2017.

Gissin, D. and Shalev-Shwartz, S. Discriminative active learning. *arXiv preprint arXiv:1907.06347*, 2019.

Grill, J., Strub, F., Altché, F., Tallec, C., Richemond, P. H., Buchatskaya, E., Doersch, C., Pires, B. Á., Guo, Z., Azar, M. G., Piot, B., Kavukcuoglu, K., Munos, R., and Valko, M. Bootstrap your own latent - A new approach to self-supervised learning. In Larochelle, H., Ranzato, M., Hadsell, R., Balcan, M., and Lin, H. (eds.), *Advances in Neural Information Processing Systems 33: Annual Conference on Neural Information Processing Systems 2020, NeurIPS 2020, December 6-12, 2020, virtual*, 2020.

Hacohen, G. and Weinshall, D. On the power of curriculum learning in training deep networks. In *International Conference on Machine Learning*, pp. 2535–2544. PMLR, 2019.

He, T., Jin, X., Ding, G., Yi, L., and Yan, C. Towards better uncertainty sampling: Active learning with multiple

views for deep convolutional neural network. In *2019 IEEE International Conference on Multimedia and Expo (ICME)*, pp. 1360–1365. IEEE, 2019.

Hong, S., Ha, H., Kim, J., and Choi, M.-K. Deep active learning with augmentation-based consistency estimation. *arXiv preprint arXiv:2011.02666*, 2020.

Joshi, A. J., Porikli, F., and Papanikolopoulos, N. Multi-class active learning for image classification. In *2009 IEEE Conference on Computer Vision and Pattern Recognition*, pp. 2372–2379. IEEE, 2009.

Kirsch, A., Van Amersfoort, J., and Gal, Y. Batchbald: Efficient and diverse batch acquisition for deep bayesian active learning. *Advances in neural information processing systems*, 32:7026–7037, 2019.

Krizhevsky, A., Hinton, G., et al. Learning multiple layers of features from tiny images. *Online*, 2009.

Kumar, M. P., Packer, B., and Koller, D. Self-paced learning for latent variable models. In *NIPS*, volume 1, pp. 2, 2010.

Le, Y. and Yang, X. Tiny imagenet visual recognition challenge. *CS 231N*, 7(7):3, 2015.

Lerner, B., Shiran, G., and Weinshall, D. Boosting the performance of semi-supervised learning with unsupervised clustering. *arXiv preprint arXiv:2012.00504*, 2020.

Lewis, D. D. and Gale, W. A. A sequential algorithm for training text classifiers. In *SIGIR’94*, pp. 3–12. Springer, 1994.

Li, X. and Guo, Y. Adaptive active learning for image classification. In *Proceedings of the IEEE Conference on Computer Vision and Pattern Recognition*, pp. 859–866, 2013.

Mahmood, R., Fidler, S., and Law, M. T. Low budget active learning via wasserstein distance: An integer programming approach. *arXiv preprint arXiv:2106.02968*, 2021.

Mittal, S., Tatarchenko, M., Çiçek, Ö., and Brox, T. Parting with illusions about deep active learning. *arXiv preprint arXiv:1912.05361*, 2019.

Munjal, P., Hayat, N., Hayat, M., Sourati, J., and Khan, S. Towards robust and reproducible active learning using neural networks. *ArXiv*, abs/2002.09564, 2020.

Nguyen, A., Yosinski, J., and Clune, J. Deep neural networks are easily fooled: High confidence predictions for unrecognizable images. In *Proceedings of the IEEE conference on computer vision and pattern recognition*, pp. 427–436, 2015.

Park, S., Han, S., Kim, S., Kim, D., Park, S., Hong, S., and Cha, M. Improving unsupervised image clustering with robust learning. In *Proceedings of the IEEE/CVF Conference on Computer Vision and Pattern Recognition*, pp. 12278–12287, 2021.

Pourahmadi, K., Nooralinejad, P., and Pirsavash, H. A simple baseline for low-budget active learning. *arXiv preprint arXiv:2110.12033*, 2021.

Ranganathan, H., Venkateswara, H., Chakraborty, S., and Panchanathan, S. Deep active learning for image classification. In *2017 IEEE International Conference on Image Processing (ICIP)*, pp. 3934–3938. IEEE, 2017.

Scheffer, T., Decomain, C., and Wrobel, S. Active hidden markov models for information extraction. In *International Symposium on Intelligent Data Analysis*, pp. 309–318. Springer, 2001.

Schröder, C. and Niekler, A. A survey of active learning for text classification using deep neural networks. *arXiv preprint arXiv:2008.07267*, 2020.

Sener, O. and Savarese, S. Active learning for convolutional neural networks: A core-set approach. In *International Conference on Learning Representations*, 2018.

Settles, B. Active learning literature survey. Computer Sciences Technical Report 1648, University of Wisconsin–Madison, 2009.

Shui, C., Zhou, F., Gagné, C., and Wang, B. Deep active learning: Unified and principled method for query and training. In *International Conference on Artificial Intelligence and Statistics*, pp. 1308–1318. PMLR, 2020.

Siméoni, O., Budnik, M., Avrithis, Y., and Gravier, G. Rethinking deep active learning: Using unlabeled data at model training. In *2020 25th International Conference on Pattern Recognition (ICPR)*, pp. 1220–1227. IEEE, 2021.

Simonyan, K. and Zisserman, A. Very deep convolutional networks for large-scale image recognition. *arXiv preprint arXiv:1409.1556*, 2014.

Sinha, S., Ebrahimi, S., and Darrell, T. Variational adversarial active learning. In *Proceedings of the IEEE/CVF International Conference on Computer Vision*, pp. 5972–5981, 2019.

Tropp, J. A. An introduction to matrix concentration inequalities. *Found. Trends Mach. Learn.*, 8(1-2):1–230, 2015. doi: 10.1561/2200000048.

Van Gansbeke, W., Vandenhende, S., Georgoulis, S., Proesmans, M., and Van Gool, L. Scan: Learning to classify

images without labels. In *European Conference on Computer Vision*, pp. 268–285. Springer, 2020.

Wang, Z., Du, B., Zhang, L., and Zhang, L. A batch-mode active learning framework by querying discriminative and representative samples for hyperspectral image classification. *Neurocomputing*, 179:88–100, 2016.

Yang, Y., Ma, Z., Nie, F., Chang, X., and Hauptmann, A. G. Multi-class active learning by uncertainty sampling with diversity maximization. *International Journal of Computer Vision*, 113(2):113–127, 2015.

Yin, C., Qian, B., Cao, S., Li, X., Wei, J., Zheng, Q., and Davidson, I. Deep similarity-based batch mode active learning with exploration-exploitation. In *2017 IEEE International Conference on Data Mining (ICDM)*, pp. 575–584. IEEE, 2017.

Yoo, D. and Kweon, I. S. Learning loss for active learning. In *Proceedings of the IEEE/CVF Conference on Computer Vision and Pattern Recognition*, pp. 93–102, 2019.

Yuan, M., Lin, H., and Boyd-Graber, J. L. Cold-start active learning through self-supervised language modeling. In Webber, B., Cohn, T., He, Y., and Liu, Y. (eds.), *Proceedings of the 2020 Conference on Empirical Methods in Natural Language Processing, EMNLP 2020, Online, November 16-20, 2020*, pp. 7935–7948. Association for Computational Linguistics, 2020.

Zhang, B., Wang, Y., Hou, W., Wu, H., Wang, J., Okumura, M., and Shinozaki, T. Flexmatch: Boosting semi-supervised learning with curriculum pseudo labeling. *CoRR*, abs/2110.08263, 2021.

Zhang, R., Isola, P., Efros, A. A., Shechtman, E., and Wang, O. The unreasonable effectiveness of deep features as a perceptual metric. In *Proceedings of the IEEE conference on computer vision and pattern recognition*, pp. 586–595, 2018.

Zhdanov, F. Diverse mini-batch active learning. *arXiv preprint arXiv:1901.05954*, 2019.

Zhu, Y., Lin, J., He, S., Wang, B., Guan, Z., Liu, H., and Cai, D. Addressing the item cold-start problem by attribute-driven active learning. *IEEE Transactions on Knowledge and Data Engineering*, 32(4):631–644, 2019.

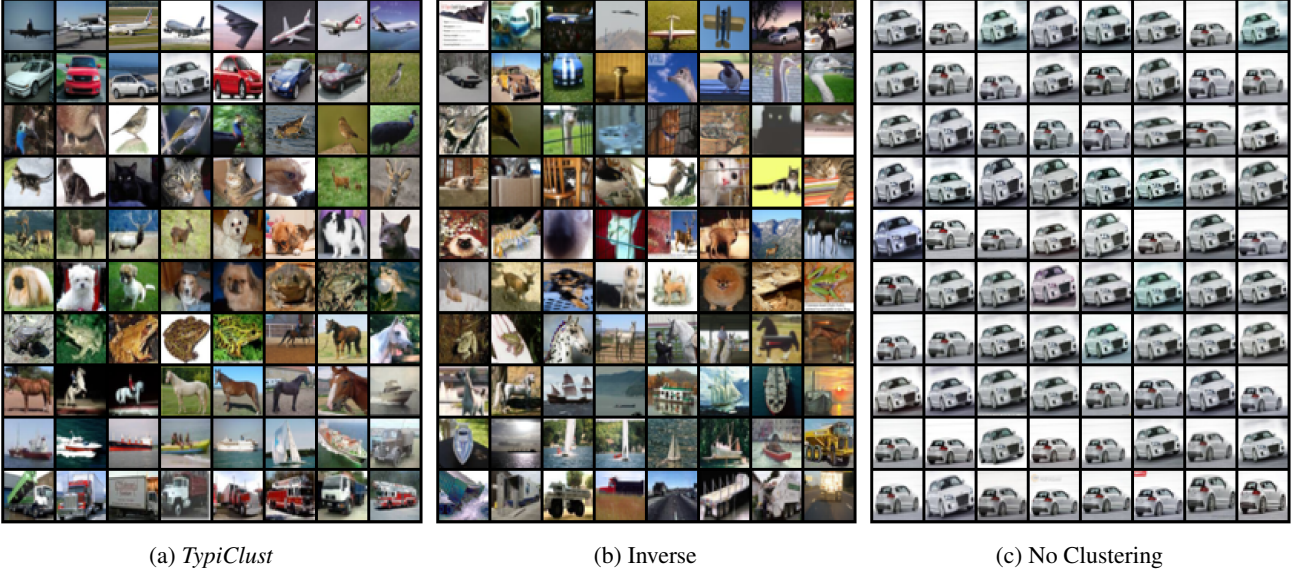


Figure 9. Qualitative measure of the importance of clustering to amplify diversity in the low budget regime on CIFAR-10. Typicality and clustering are calculated on the penultimate layer of SimCLR feature space.

Appendix

A. Visualization of Query Selection Method

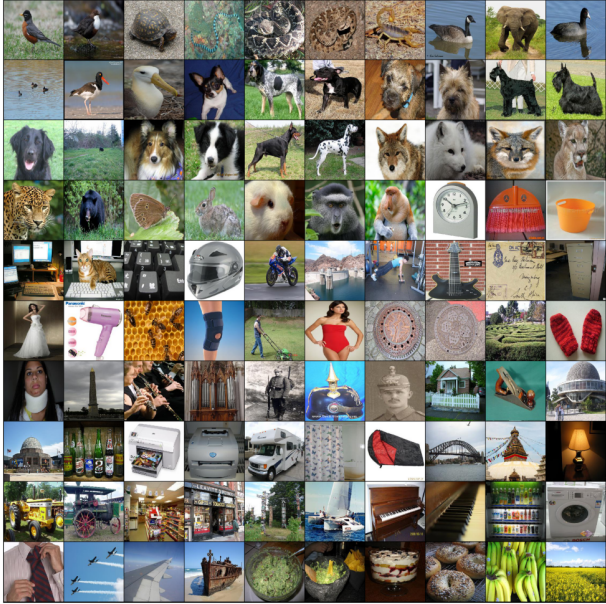


Figure 10. 100 ImageNet-100 examples selected by *TypiClust*.

A.1. The Importance of Diversity and Typicality

Fig. 9 compares the selection of 80 images according to three selection strategies on CIFAR10: (a) Clustering the feature space to 80 clusters, and selecting most typical ex-

ample from each cluster. (b) Clustering the feature space to 80 clusters, and selecting least typical example from each cluster. (c) Greedy selection of the 80 densest examples.

Specifically, Fig. 9a shows the selection of *TypiClust*, which selects diverse samples that are easy to recognize visually. Fig. 9b shows the selection of the least typical examples from every cluster, which are harder to recognize visually. Fig. 9c shows the most typical examples, selected without clustering. The selected examples are highly correlated, and often appear to be different variants of the same image.

A.2. Visualizing the Selected Examples

For visualization, Fig. 10 shows the 100 ImageNet examples selected by *TypiClust* from ImageNet-100. We further visualize our strategy’s selection criteria, by demonstrating the selection of 30 examples from CIFAR-10 in greater detail. *TypiClust* first clusters the dataset to 30 clusters - using SCAN clustering algorithm. Fig. 11 plots the tSNE dimensionality reduction of the model’s feature space, colored in various ways: Fig. 11a shows the tSNE embedding colored by the GT labels. Fig. 11b shows the tSNE embedding colored by the cluster assignment. Fig. 11c shows the tSNE embedding colored by the log density (for better visualization). Examples marked with \times are selected for labeling. Fig. 11d shows that the actual images thus selected.

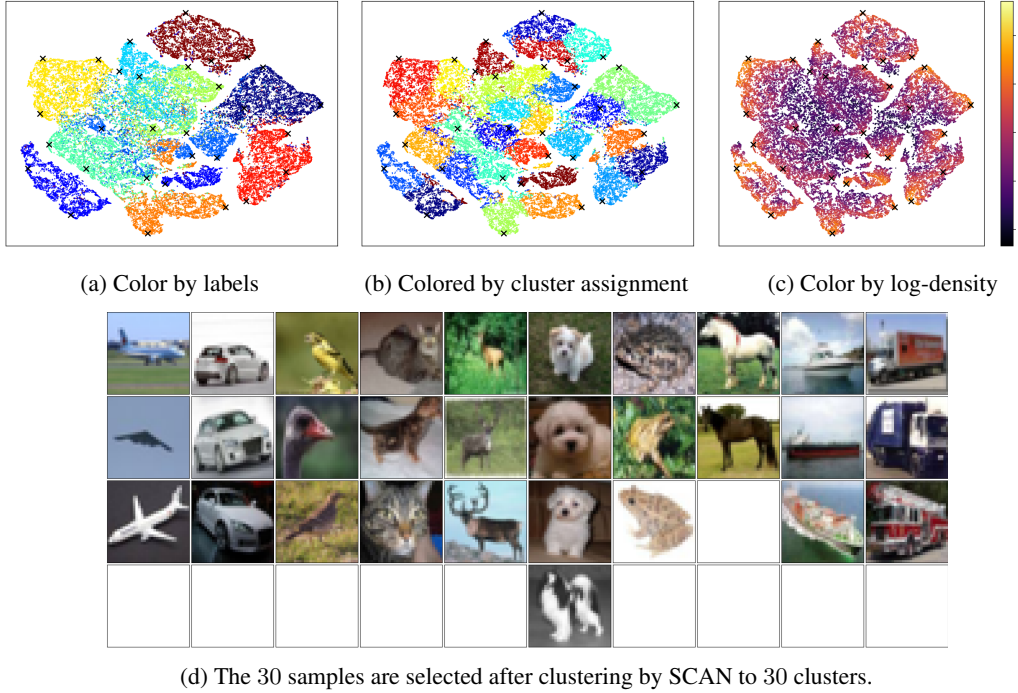


Figure 11. Visualization of the selection of 30 examples using SCAN clustering algorithm - examples marked with \times are selected for labeling. (d) The selected images, each column represents a different label.

B. Mixture Model Lemmas and Proofs

B.1. Proof of Thm. 1

Theorem 1. Let $0 < p < 1$, $0 < \alpha < \frac{p}{1-p}$ denote some constants. Given error score $E(x)$, the following threshold test decreases the expected error for sample

$$\frac{E'(pm)}{E'(\alpha(1-p)m)} \begin{cases} > \frac{\alpha(1-p)}{p} & \Rightarrow \text{over sample region } R_1 \\ < \frac{\alpha(1-p)}{p} & \Rightarrow \text{over sample region } R_2 \end{cases}$$

Proof. In Section 2.1.2 we define this biased sampling strategy:

$$\begin{aligned} m_1 &= p \cdot m + \Delta \\ m_2 &= (1-p) \cdot m - \Delta \end{aligned} \tag{7}$$

Here, region R_1 is over-sampled when $\Delta > 0$, and vice versa. Starting from (3), we obtain the test whereby the

error score $E_{\mathcal{D}}(m)$ decreases when $\Delta > 0$:

$$\begin{aligned} & p \cdot E(p \cdot m + \Delta) + (1-p) \cdot E(\alpha((1-p)m - \Delta)) \\ & < p \cdot E(p \cdot m) + (1-p) \cdot E(\alpha(1-p)m) \\ \Rightarrow & (1-p)[E(\alpha(1-p)m) - E(\alpha((1-p)m - \Delta))] \\ & > p[E(p \cdot m + \Delta) - E(p \cdot m)] \\ \Rightarrow & \alpha(1-p) \frac{E(\alpha(1-p)m) - E(\alpha(1-p)m - \alpha\Delta)}{\alpha\Delta} \\ & > p \frac{E(p \cdot m + \Delta) - E(p \cdot m)}{\Delta} \end{aligned}$$

Since $E(x)$ is differentiable and strictly monotonically decreasing with $E' < 0$, in the limit of infinitesimal Δ

$$\frac{E'(pm)}{E'(\alpha(1-p)m)} > \frac{\alpha(1-p)}{p}$$

The proof for $\Delta < 0$ is similar. \square

B.2. Undulating Error Score: Sufficient Conditions

In this section, we provide proof for Thm. 2, which is stated in Section 2.2. The theorem provides sufficient conditions for error scores to be undulating (see Def. 2). We start with a few lemmas which will be used in this proof.

Lemma 1. Let $f : \mathbb{R}^+ \rightarrow \mathbb{R}$ denote a differentiable function

with $f(0) \neq 0$. Then

$$\lim_{x \rightarrow 0^+} \frac{f(x)}{f(ax)} = 1 \quad \forall a \in (0, 1)$$

Lemma 2. Let $F : \mathbb{R}^+ \rightarrow \mathbb{R}_*^+$ and $f = F'$ denote a positive differentiable strictly monotonically decreasing function ($F > 0, f < 0$). Assume that $\lim_{x \rightarrow \infty} F(x) = 0$, and that the limits $\lim_{x \rightarrow \infty} \frac{F(x)}{F(ax)}, \lim_{x \rightarrow \infty} \frac{f(x)}{f(ax)}$ exist $\forall a \in (0, 1)$. Denote $g(x) = -\ln(F(x))$. If

$$g'(x) = \omega\left(\frac{1}{x}\right)$$

then:

$$\lim_{x \rightarrow \infty} \frac{f(x)}{f(ax)} = 0 \quad \forall a \in (0, 1)$$

Proof. We can write $F(x) = e^{-g(x)}$. It follows from the mean value theorem that $\exists t$ $ax < t < x$, such that:

$$\begin{aligned} \frac{F(x)}{F(ax)} &= e^{-(g(x) - g(ax))} \\ &= e^{-(g'(t)x(1-a))} \\ &= e^{-(g'(t)t \cdot \frac{x}{t} \cdot (1-a))} \end{aligned}$$

Since $g'(x) = \omega\left(\frac{1}{x}\right)$, we get:

$$\lim_{t \rightarrow \infty} t \cdot g'(t) = \infty$$

As $(1-a) < \frac{x}{t}(1-a) < \frac{(1-a)}{a}$, it follows that:

$$\lim_{x \rightarrow \infty} \frac{F(x)}{F(ax)} = 0$$

From the assumption that the limits exist, and since $\lim_{x \rightarrow \infty} F(x) = \lim_{x \rightarrow \infty} F(ax) = 0$, we can use L'Hôpital's rule and get:

$$\lim_{x \rightarrow \infty} \frac{F(x)}{F(ax)} = \lim_{x \rightarrow \infty} \frac{f(x)}{af(ax)} = \frac{1}{a} \lim_{x \rightarrow \infty} \frac{f(x)}{f(ax)} = 0$$

□

Lemma 3. Let $F : \mathbb{R}^+ \rightarrow \mathbb{R}_*^+$ denote a positive differentiable function ($F > 0$). Denote $g(x) = -\ln(F(x))$. Assume that $\lim_{x \rightarrow \infty} g'(x)$ exists, and

$$g(x) = \omega(\log(x))$$

Then

$$g'(x) = \omega\left(\frac{1}{x}\right)$$

Proof. $g(x) = \omega(\log(x))$ implies that

$$\lim_{x \rightarrow \infty} \frac{g(x)}{\ln(x)} = \infty, \quad \lim_{x \rightarrow \infty} g(x) = \infty$$

We can now use L'Hôpital's rule and get:

$$\infty = \lim_{x \rightarrow \infty} \frac{g(x)}{\ln(x)} = \lim_{x \rightarrow \infty} \frac{g'(x)}{\frac{1}{x}} = \lim_{x \rightarrow \infty} xg'(x)$$

□

Theorem 2. Let $0 < p < 1, 0 < \alpha < \frac{p}{1-p}$ denote some constants. Error score $E(x)$ is undulating if the following assumptions hold:

1. $E(x)$ is a proper error score (see Def. 4)
2. $\lim_{x \rightarrow \infty} \frac{E'(x)}{E(x)}, \lim_{x \rightarrow \infty} \frac{E(x)}{E(ax)}, \lim_{x \rightarrow \infty} \frac{E'(x)}{E'(ax)}$ exist $\forall a \in (0, 1)$
3. $-\log(E(x)) = \omega(\log(x))$

Proof. We define $f(x) = -E'(px), a = \frac{\alpha(1-p)}{p} < 1$. From assumption (1) and using Lemma 1, we get:

$$\lim_{x \rightarrow 0^+} \frac{E'(px)}{E'(\alpha(1-p)x)} = 1$$

Therefore there exists some $z_1 \in \mathbb{R}^+$ such that $\forall x < z_1$:

$$\frac{E'(px)}{E'(\alpha(1-p)x)} > \frac{\alpha(1-p)}{p}$$

From assumptions (1-3) and using Lemmas 2-3, we get:

$$\lim_{x \rightarrow \infty} \frac{E'(x)}{E'(ax)} = \lim_{x \rightarrow \infty} \frac{E'(px)}{E'(\alpha(1-p)x)} = 0$$

and therefore there is some $z_2 \in \mathbb{R}^+$ such that $\forall x > z_2$:

$$\frac{E'(px)}{E'(\alpha(1-p)x)} < \frac{\alpha(1-p)}{p}$$

From Def. 2 we get that $E(x)$ is undulating. □

B.3. SP-undulating Error Score: Sufficient Conditions

In this section, we provide proof for Thm. 3, which is stated in Section 2.2.2. It provides sufficient conditions for error scores to be SP-undulating (see Def. 2), extending Thm. 2. We start with a few lemmas which will be used in this proof.

Lemma 4. Let $f : \mathbb{R}^+ \rightarrow \mathbb{R}_*^+$ denote a positive differentiable function ($f > 0$). Let $0 < a < 1$ denote some constant. If

$$h(x) = \frac{-f'(x)x}{f(x)}$$

is strictly monotonically increasing, then

$$g(x) = \frac{f(x)}{f(ax)}$$

is strictly monotonically decreasing.

Proof. $g(x)$ is monotonically decreasing iff $g'(x) < 0$, where

$$g'(x) = \frac{f'(x)f(ax) - af(x)f'(ax)}{f(ax)^2}$$

This condition translates to:

$$f'(x)f(ax) - af(x)f'(ax) < 0$$

As by assumption $h(x)$ is monotonically increasing and $h(ax) < h(x)$, we get that $\forall x > 0$:

$$\begin{aligned} \frac{-f'(ax)ax}{f(ax)} &< \frac{-f'(x)x}{f(x)} \\ \implies \frac{-f'(ax)a}{f(ax)} &< \frac{-f'(x)}{f(x)} \\ \implies -f'(ax)f(x)a &< -f'(x)f(ax) \end{aligned}$$

□

Lemma 5. Let $f : \mathbb{R}^+ \rightarrow \mathbb{R}_*^+$ denote a positive differentiable log-concave function which is strictly monotonically decreasing ($f > 0, f' < 0, (\log(f))'' \leq 0$). Then the following function is strictly monotonically increasing:

$$h(x) = \frac{-f'(x)x}{f(x)}$$

Proof. $h(x)$ is strictly monotonically increasing iff $h'(x) > 0$, which holds iff:

$$\begin{aligned} h'(x) &= \frac{xf'(x)^2 - xf(x)f''(x) - f(x)f'(x)}{f(x)^2} > 0 \\ \implies x[f'(x)^2 - f(x)f''(x)] - f(x)f'(x) &> 0 \end{aligned}$$

Recall that $x > 0$ and $-f(x)f'(x) > 0 \forall x \in \mathbb{R}^+$. Since f is log-concave, we also have that $f'(x)^2 - f(x)f''(x) \geq 0$, which concludes the proof. □

Theorem 3. Let $0 < p < 1, 0 < \alpha < \frac{p}{1-p}$ denote some constants. Error score $E(x)$ is SP-undulating if the following assumptions hold:

1. $E(x)$ is an undulating proper error score.
2. At least one of the following conditions holds:
 - (a) $\frac{-E''(x) \cdot x}{E'(x)}$ is monotonically increasing with x .
 - (b) $-E'(x)$ is strictly monotonic decreasing and log-concave.

Proof. Define the following positive continuous function

$$H(x) = \frac{E'(px)}{E'(\alpha(1-p)x)}$$

Let $f(x) = -E'(x)$, $a = \frac{a(1-p)}{p} < 1$. Note that assumption (2a) follows from assumption (2b) and Lemma 5. Assumption (2) therefore implies that $\frac{-f'(x)x}{f(x)}$ is strictly monotonically increasing, and by Lemma 4 we can conclude that $H(x)$ is monotonically decreasing. Together with assumption (1), $H(x) = \frac{\alpha(1-p)}{p}$ at a single point, and we may therefore conclude that $E(x)$ is SP-undulating. □

Corollary 3. If p - the probability of region R_1 - is sufficiently small so that $p < \frac{\alpha}{1+\alpha}$, then the conclusions are reversed: it is beneficial to initially favor the hard to learn region R_2 , and favor R_1 only towards the end of training.

C. Error Function of Simple Mixture Models

C.1. Mixture of Two Linear Classifiers

In this section, we provide proofs for Thm. 4 and Thm. 5, which are stated in Section 2.3.1. Thm. 4 provides a bound on the error score of a single linear classifier, showing that under mild conditions, this score is bounded by an exponentially decreasing function in the number of training examples m_j . Thm. 5 states conditions under which the error score of a mixture of two linear models $E(m)$ is undulating, thus depicting the phase-transition behavior.

Bounding the error of each mixture component. Henceforth we use the notations of Section 2.3.1, where for clarity, m_j is replaced by m while we are discussing the bound on a single component j . Let \mathbf{x}_i denote the i -th data point and i -th column of X . Let μ_1 and μ_2 denote the respective means of the two classes, and $\mu = \mu_1 - \mu_2$ denote the vector difference between the means.

Assuming that the data is normalized to 0 mean, the maximum likelihood estimators for the covariance matrix of the distribution Σ and class means, denoted $\hat{\Sigma}$ and $\hat{\mu}_1, \hat{\mu}_2$ respectively, are the following:

$$\hat{\Sigma} = \frac{1}{m} \sum_{i=1}^m \mathbf{x}_i \mathbf{x}_i^\top = \frac{1}{m} \mathbf{X} \mathbf{X}^\top \quad (8)$$

$$\hat{\mu}_j = \frac{1}{m_j} \sum_{\mathbf{x}_i \in C_j} \mathbf{x}_i \implies \mathbf{y} \mathbf{X}^\top = m_1 \hat{\mu}_1 - m_2 \hat{\mu}_2 \quad (9)$$

where C_j denotes the set of points in class $j \in [2]$. Thus, the ML linear separator can be written as:

$$\begin{aligned} \hat{\mathbf{w}} &= \mathbf{y} \mathbf{X}^\top (\mathbf{X} \mathbf{X}^\top)^{-1} \\ &= [m_1 \hat{\mu}_1 - m_2 \hat{\mu}_2] (m \hat{\Sigma})^{-1} = \hat{\mu} \hat{\Sigma}^{-1} \end{aligned}$$

where $\hat{\mu} = \frac{1}{m} \mathbf{y} \mathbf{X}^\top$. Note that $\hat{\mu}$ is the sample mean of vectors $\{y_i \mathbf{x}_i\}_{i=1}^m$, and $\hat{\Sigma}$ is the sample covariance of $\{\mathbf{x}_i\}_{i=1}^m$.

When $d > m$ (fewer training points than the input space dimension), $\hat{\Sigma}$ is rank deficient and therefore $\hat{\Sigma}^{-1}$ is not defined. Moreover, the solution is not unique. Nevertheless, it

can be shown that the minimal norm solution is the Penrose pseudo-inverse $\hat{\Sigma}^+$, where

$$\hat{\Sigma} = UDU^\top \implies \hat{\Sigma}^+ = U D^{-1} U^\top$$

and using the notations

$$\begin{aligned} D &= \text{diag}(d_1, \dots, d_m, 0, \dots, 0) \\ D^{-1} &= \text{diag}(d_1^{-1}, \dots, d_m^{-1}, 0, \dots, 0) \end{aligned}$$

Ignoring the question of uniqueness, estimating \mathbf{w} is therefore reduced to evaluating the estimators in (8) and (9). These ML estimators have the following known upper bounds on their error:

1. Bounding $\hat{\Sigma}$: from known results on covariance estimation (Tropp, 2015), using Bernstein matrix inequality

$$P(\|\hat{\Sigma} - \Sigma\|_{op} \geq t) \leq 2de^{-amt^2} \quad (10)$$

Constant a does not depend on m ; it is determined by the assumed bound on the L_2 norm of vectors \mathbf{x}_i , and the norm of the true covariance matrix Σ .

2. Bounding $\hat{\mu}$: by Hoeffding's inequality, we have that $P(|\hat{\mu}_k - \mu_k| \geq t) \leq e^{-2mt^2} \forall k \in [d]$. Thus

$$\begin{aligned} P(\|\hat{\mu} - \mu\| \geq t) &= P(\|\hat{\mu} - \mu\|^2 \geq t^2) \\ &= P\left(\sum_{k=1}^d |\hat{\mu}_k - \mu_k|^2 \geq t^2\right) \\ &\leq \sum_{k=1}^d P\left(|\hat{\mu}_k - \mu_k|^2 \geq \frac{t^2}{d}\right) \quad (11) \\ &= \sum_{k=1}^d P\left(|\hat{\mu}_k - \mu_k| \geq \frac{t}{\sqrt{d}}\right) \\ &\leq de^{-2m\frac{t^2}{d}} \end{aligned}$$

The first inequality follows from the union-bound inequality.

Theorem 4. Assume: (i) a bounded sample $\|\mathbf{x}_i\| \leq B$, where X is sufficiently far from singular so that its smallest positive singular value is bounded from below by $\frac{1}{\Lambda}$; (ii) a realizable binary problem where the classes are separable by margin δ ; (iii) full rank data covariance, where $\frac{1}{\lambda}$ denotes its smallest singular value. Then there exist some positive constants $k, \nu > 0$, such that $\forall m_j \in \mathbb{N}$ and every sample \mathbb{X}^{m_j} , the expected error of $\hat{\mathbf{w}}$ obtained using \mathbb{X}^{m_j} is bounded by:

$$F(m_j) = \mathbb{E}_{\mathbf{X} \sim \mathcal{D}_j} [0 - 1 \text{ loss of } \hat{\mathbf{w}}] \leq ke^{-\nu m_j} \quad (12)$$

Proof. It follows from our assumptions that $\|\hat{\Sigma}^+\|_{op} \leq \Lambda$. An error will occur at $\mathbf{x} \in C_1$ if $\mathbf{w}_{opt}^\top \mathbf{x} \geq \delta$ and $\hat{\mathbf{w}}^\top \mathbf{x} < 0$,

and vice versa for $\mathbf{x} \in C_2$. In either case, the difference between the predictions of \mathbf{w}_{opt} and $\hat{\mathbf{w}}$ deviate by more than δ . Thus

$$\begin{aligned} F(m) &= \mathbb{E}_{\mathbf{X} \sim \mathcal{D}} [0 - 1 \text{ loss}] = P(\text{error}) \\ &\leq P\left(\left|\mu^\top \Sigma^{-1} \mathbf{x} - \hat{\mu}^\top \hat{\Sigma}^+ \mathbf{x}\right| > \delta\right) \quad (13) \end{aligned}$$

Invoking the triangular inequality

$$\begin{aligned} \Delta &= \left|\mu^\top \Sigma^{-1} \mathbf{x} - \hat{\mu}^\top \hat{\Sigma}^+ \mathbf{x}\right| \\ &= \left|(\mu - \hat{\mu})^\top \Sigma^{-1} \mathbf{x} + \hat{\mu}^\top (\Sigma^{-1} - \hat{\Sigma}^+) \mathbf{x}\right| \quad (14) \\ &\leq \left|(\mu - \hat{\mu})^\top \Sigma^{-1} \mathbf{x}\right| + \left|\hat{\mu}^\top (\Sigma^{-1} - \hat{\Sigma}^+) \mathbf{x}\right| \end{aligned}$$

Before proceeding, we need to get from $(\Sigma^{-1} - \hat{\Sigma}^+)$ to $(\Sigma - \hat{\Sigma})$, for which we have established a bound. Because $\hat{\Sigma} \in \mathbb{R}^{d \times d}$ is of rank m , $Q = \hat{\Sigma}^+ \hat{\Sigma} = U \text{diag}(1, \dots, 1, 0, \dots, 0) U^\top$ is a projection matrix of rank m , projecting vectors to the subspace spanned by the training set $\{\mathbf{x}_i\}_{i=1}^m$. Thus $Q\hat{\mu} = \hat{\mu}$. Additionally, by definition, $\hat{\Sigma}^+ \hat{\Sigma} \hat{\Sigma}^+ = \hat{\Sigma}^+$ and Q is symmetric. It follows that

$$\hat{\mu}^\top (\Sigma^{-1} - \hat{\Sigma}^+) \mathbf{x} = \hat{\mu}^\top (Q \Sigma^{-1} - \hat{\Sigma}^+) \mathbf{x}$$

while

$$\hat{\Sigma}^+ (\hat{\Sigma} - \Sigma) \Sigma^{-1} = Q \Sigma^{-1} - \hat{\Sigma}^+$$

Together

$$\hat{\mu}^\top [\Sigma^{-1} - \hat{\Sigma}^+] \mathbf{x} = \hat{\mu}^\top [\hat{\Sigma}^+ (\hat{\Sigma} - \Sigma) \Sigma^{-1}] \mathbf{x} \quad (15)$$

Inserting (15) back into (14)

$$\begin{aligned} \Delta &\leq \|\mu - \hat{\mu}\| \|\Sigma^{-1}\|_{op} \|\mathbf{x}\| \\ &\quad + \|\hat{\mu}\| \|\hat{\Sigma}^+\|_{op} \|\hat{\Sigma} - \Sigma\|_{op} \|\Sigma^{-1}\|_{op} \|\mathbf{x}\| \\ &\leq \|\mu - \hat{\mu}\| \lambda B + B \Lambda \|\hat{\Sigma} - \Sigma\|_{op} \lambda B \end{aligned}$$

It follows that

$$\begin{aligned} P\left(\left|\mu^\top \Sigma^{-1} \mathbf{x} - \hat{\mu}^\top \hat{\Sigma}^+ \mathbf{x}\right| > \delta\right) &\leq P(\|\mu - \hat{\mu}\| \lambda B + \|\hat{\Sigma} - \Sigma\|_{op} \lambda \Lambda B^2 > \delta) \\ &\leq P(\|\mu - \hat{\mu}\| \lambda B > \frac{\delta}{2}) + P(\|\hat{\Sigma} - \Sigma\|_{op} \lambda \Lambda B^2 > \frac{\delta}{2}) \\ &\leq de^{-2m(\frac{\delta}{2\lambda B})^2} + 2de^{-km(\frac{\delta}{2\lambda \Lambda B^2})^2} \\ &\leq 3de^{-k'm\delta^2} \end{aligned}$$

The second transition follows from the union bound inequality, and the third from (10)-(11), where:

$$k' = \min \left\{ \frac{2}{d} \left(\frac{1}{2\lambda B} \right)^2, a \left(\frac{1}{2\lambda \Lambda B^2} \right)^2 \right\}$$

□

A mixture classifier. Assume a mixture of two linear classifiers, and let $E(m) = p \cdot E_{\mathcal{D}_1}(m_1) + (1 - p) \cdot E_{\mathcal{D}_2}(m_2)$ denote its error score.

Theorem 5. *Keep the assumptions stated in Thm. 4, and assume in addition that $\forall a \in (0, 1)$, $\exists \lim_{m \rightarrow \infty} \frac{E'(m)}{E(m)}$, $\lim_{m \rightarrow \infty} \frac{E(m)}{E(am)}$ $\lim_{m \rightarrow \infty} \frac{E'(m)}{E'(am)}$. Then the error score of a mixture of two linear classifiers is undulating.*

Proof. In each region j of the mixture, Thm. 4 implies that its corresponding error score as defined in Def. 1

$$E_{\mathcal{D}_j}(m_j) = \mathbb{E}_{\mathbb{X}^{m_j} \sim \mathcal{D}_j^{m_j}} [F(m_j)]$$

is bounded by an exponentially decreasing function of m_j . Since $E_{\mathcal{D}_j}(m_j)$ measures the expected error over all samples of size m_j , it can also be shown that $E_{\mathcal{D}_j}(m_j)$ is monotonically decreasing with m_j . From the separability assumption, $\lim_{m_j \rightarrow \infty} E_{\mathcal{D}_j}(m_j) = 0$. Finally, since $E(m)$ is a linear combination of two such functions, it also has these properties. We, therefore, conclude from Cor. 1 that the error score of a mixture of two linear classifiers is undulating. \square

C.2. 1-NN Classifier

If the training sample size m is small, our analysis shows that under certain circumstances, it is beneficial to prefer sampling from a region R where $E_{\mathcal{D}_R}(m) < E_{\mathcal{D}_{\Omega \setminus R}}(m)$. We now show that the set of densest points has this property.

To this end, we adopt the one-Nearest-Neighbor (1-NN) classification framework. This is a natural framework to address the aforementioned question for two reasons: (i) It involves a general classifier with desirable asymptotic properties. (ii) The computation of both class density and 1-NN is governed by local distances in the input feature space.

To begin with, assume a classification problem with k classes that are separated by at least ρ . More specifically, assume that $\forall \mathbf{x}, \mathbf{x}' \in \mathbb{R}^d$, if $\|\mathbf{x}' - \mathbf{x}\| \leq \rho$ then $y' = y$. Let $B_v(\mathbf{x}_i, r)$ denote a ball centered at $\mathbf{x}_i \in \mathbb{R}^d$, with radius smaller than r and volume v . For $\mathbf{X} = (\mathbf{x}, y)$, let $f_{\mathcal{D}}(\mathbf{X})$ denote the density function from which data is drawn when sampling is random (and specifically at test time).

Assume a 1-NN classifier whose training sample is $T = \{\mathbf{x}_i, y_i\}_{i=1}^m$, and whose prediction at $\mathbf{X} = (\mathbf{x}, y)$ is

$$y = \begin{cases} y_{\nu}, & \nu = \arg \min_{i \in [m]} \|\mathbf{x} - \mathbf{x}_i\| \\ y \sim U(1, k) & \text{otherwise} \end{cases} \quad \mathbf{x} \in B_v(\mathbf{x}_i, \rho)$$

The error probability of this classifier at \mathbf{x} is

$$P(x) = \begin{cases} 0 & \exists i \text{ such that } \mathbf{x} \in B_v(\mathbf{x}_i, \rho) \\ \frac{k-1}{k} & \text{otherwise} \end{cases}$$

The $0 - 1$ loss of this classifier is

$$\mathbb{E}_{\mathbf{X} \sim \mathcal{D}}[P(x)] = \frac{k-1}{k} \text{Prob} \left[\mathbf{x} \notin \bigcup_{i=1}^m B_v(\mathbf{x}_i, \rho) \right] \quad (16)$$

where $B_v(\mathbf{x}_i, r)$ denotes a ball centered at $\mathbf{x}_i \in \mathbb{R}^d$, with radius smaller than r and volume v .

The next theorem states properties of set T which are beneficial to the minimization of this loss:

Theorem 6. *Let A_i denote the event $\{\mathbf{x} \in B_v(\mathbf{x}_i, r)\}$, and assume that these events are independent. Then we have*

$$L(T) = \frac{k-1}{k} \left[1 - \sum_{i=1}^m f_{\mathcal{D}}(\mathbf{X}_i)v + O(v^2) \right]$$

Proof. Using the independence assumption and (16), and assuming that v is sufficiently small

$$\begin{aligned} L(T) &= \frac{k-1}{k} \left[1 - P \left(\bigcup_{i=1}^m A_i \right) \right] \\ &= \frac{k-1}{k} \left[1 - \sum_{i=1}^m P(A_i) \right] \\ &= \frac{k-1}{k} \left[1 - \sum_{i=1}^m \int_{\mathbf{X}} \mathbb{1}_{\mathbf{x} \in B_v(\mathbf{x}_i, r)} f_{\mathcal{D}}(\mathbf{X}) d\mathbf{X} \right] \\ &= \frac{k-1}{k} \left[1 - \sum_{i=1}^m f_{\mathcal{D}}(\mathbf{X}_i)v + O(v^2) \right] \end{aligned}$$

\square

In Thm. 6, we show that if v is sufficiently small, the 0-1 loss is minimized when choosing a set of independent points $\{\mathbf{X}_i\}_{i=1}^m$ that maximizes $\sum_{i=1}^m f_{\mathcal{D}}(\mathbf{X}_i)$. This suggests that the selection of an initial pool of size m will benefit from the following heuristic:

- **Max density:** when selecting a point \mathbf{X}_i , maximize its density $f_{\mathcal{D}}(\mathbf{X}_i)$.
- **Diversity:** select varied points, for which the events $\{\mathbf{x} \in B_v(\mathbf{x}_i, \rho)\}$ are approximately independent.

D. Theoretical Analysis: Visualization

D.1. Linear and Concave Error Functions

Fig. 12 illustrates that if the *error score* is concave or linear, over sampling from R_1 is **always** beneficial, as $\frac{E'(pm)}{E(\alpha(1-p)m)} \geq 1 > \frac{\alpha(1-p)}{p}$. Such functions are never undulating.

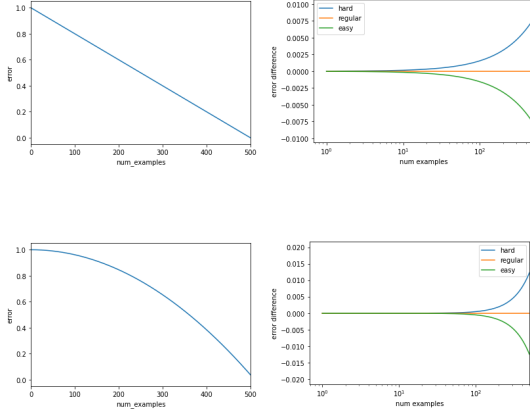


Figure 12. Plotting the generalization error of the mixture model given $p = 0.8, \alpha = 0.1, q = 0.01$ for linear error score (top) and concave error score (bottom). In the left panels, we see a visualization of the error scores, and on the right panels, we see the corresponding generalization error as a function of the number of examples. We see that over-sampling from R_1 is always beneficial in these cases.

D.2. Mixture of Two Linear Models

We now empirically analyze the error score function of the mixture of two linear classifiers, defined in Section 2.3.1. Each linear classifier is trained on a different area of the support. The data is 100 dimensional, linearly separable in each region. The margin is used to determine the α of the data. The data is chosen such that $p = 0.9, \alpha = 0.2$. The results are shown in Fig. 13.

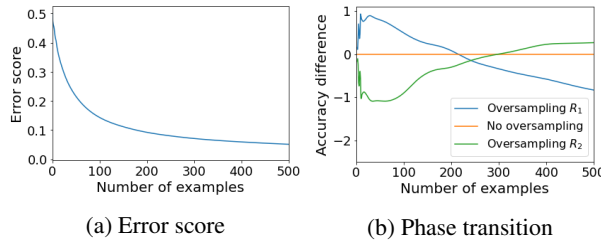


Figure 13. (a) The error score $E(m)$ as a function of the number of examples, averaged over 10k repetitions. While the error score is not exponential, it could be upper bounded by an exponential function, as analytically shown in Section 2.3.1. (b) The differences in accuracy when over-sampling from either R_1 and R_2 over a random sampling from the data distribution. Although the error score is only proven to be undulating, we can see that in practice it is also SP-undulating.

D.3. Error Scores of Deep Neural Networks

Next, we plot the error scores of deep neural networks on image classification tasks. In all datasets we tried, the error of deep networks as a function of the number of examples drops much faster than an exponential function and therefore

can be shown to be undulating. In practice, such error functions are also SP-undulating. To see some examples of these error functions in super-classes of CIFAR-100, refer to Fig. 14.

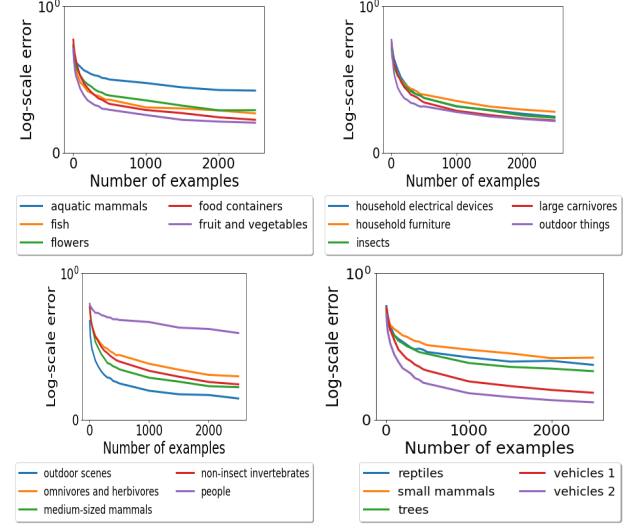


Figure 14. Log-error scores of image classification datasets as a function of the number of training examples. Each score is calculated as $1 - \text{accuracy}$, averaged on 100 VGG-16 networks trained on super-classes of CIFAR-100. Each line represents the error of a different super-class. As the log of the error is plotted, it can be seen that in all cases the error scores are monotonic decreasing and can be bounded above by some exponential function, suggesting that many of the assumptions in Thm. 3 hold.

E. Implementation Details

E.1. Code for Our Suggested Strategy

Algorithm 1 *TypiClust* initial pooling algorithm

```

Input: Unlabeled pool  $U$ , Budget  $B$ , Number of neighbors  $k$ 
Output:  $B$  typical and diverse examples to query
Embedding  $\leftarrow$  Representation_Learning( $U$ )
Data_clusters  $\leftarrow$  Clustering_algorithm(Embedding,  $B$ )
Sort Data_clusters by cluster size
Queries  $\leftarrow \emptyset$ 
for all  $i = 1, \dots, B$  do
     $I \leftarrow \{x_i \in U \mid i \in \text{Data\_clusters}[i]\}$ 
     $\text{Typ} \leftarrow \left\{ \left( \sum_{x_j \in KNN(x_i)} \|x_i - x_j\|_2 \right)^{-1} \mid x_i \in I \right\}$ 
    Add  $\arg \max(\text{Typ})$  to Queries
end for
return Queries

```

Alg. 1 provides pseudo-code for our suggested initial sam-

pling strategy, as described in Section 3.

E.2. Method Implementation Details

Step 1: Representation learning - CIFAR and TinyImageNet. We trained SimCLR using the code provided by [Van Gansbeke et al. \(2020\)](#) for CIFAR-10, CIFAR-100 and TinyImageNet. Specifically, we used ResNet18 with an MLP projection layer to a 128 vector, trained for 500 epochs. All the training hyper-parameters were identical to those used by SCAN. After training, we used the 512 dimensional penultimate layer as the representation space. As in SCAN, we used an SGD optimizer with 0.9 momentum, and initial learning rate of 0.4 with a cosine scheduler. The batch size was 512 and weight decay of 0.0001. The augmentations were random resized crops, random horizontal flips, color jittering, and random grayscaling. We refer to [Van Gansbeke et al. \(2020\)](#) for additional details. We used the L2 normalized penultimate layer as embedding.

Step 1: Representation learning - ImageNet. We extracted embedding from the official (ViT-S/16) DINO weights pre-trained on ImageNet. We used the L2 normalized penultimate layer as embedding.

Step 2: Clustering for diversity. We limit the number of clusters when partitioning the data to $max_clusters$ (a hyper-parameter). This parameter was arbitrarily picked as 500 for CIFAR-10 and CIFAR-100 and 1000 for TinyImageNet (other values resulted in similar behavior). This is done for two reasons: (a) prevent over clustering (and having too small clusters); (b) stabilize clustering algorithms. The number of clusters chosen is $K = \min(|L_{i-1}| + B, max_clusters)$.

K-Means. We used scikit-learn KMeans when $K \leq 50$ and MiniBatchKMeans otherwise. This was done to reduce runtime when the number of clusters is large.

SCAN. We used the code provided by SCAN and modified the number of clusters to K . We only trained the first step of SCAN (we did not perform the pseudo labeling step, since it degraded clustering performance).

Step 3: Clustering for diversity. Since we introduced $max_cluster$, we are no longer guaranteed to have B clusters that don't intersect the labeled set. Moreover, to estimate typicality, we require > 20 samples in every cluster. To solve this, we use $\min\{20, cluster_size\}$ nearest neighbors. To avoid inaccurate estimation of the typicality, we drop clusters with less than 5 samples².

Therefore, we add points iteratively until the budget is exhausted, in the following way: (1) Out of the clusters with

²This limiting case was rarely encountered, as clusters are usually balanced.

the fewest labeled points and of size larger than 5, select the largest cluster. (2) Compute the Typicality of every point in the selected cluster, using $\min\{20, cluster_size\}$ neighbors. (3) Add to the query the point with the highest typicality.

E.3. Evaluation and Implementation Details

E.3.1. FULLY SUPERVISED EVALUATION

We used the active learning comparison framework by [Munjal et al. \(2020\)](#). Specifically, we trained a ResNet18 on the labeled set, optimizing using SGD with 0.9 momentum and Nesterov momentum. The initial learning rate is 0.025 and was modified using a cosine scheduler. The augmentations used are random crops and horizontal flips. Our changes to this framework are listed below.

Re-Initialize weights between iterations When training with extremely low budgets, networks tend to produce over-confident predictions. Therefore, when querying samples and fine-tuning from the existing model, the loss tends to "spike", which leads to optimization issues. Therefore, we re-initialize the weights between iterations.

TinyImageNet modifications As training did not converge in the original implementation over Tiny-ImageNet, we increased the number of epochs from 100 to 200 and changed the minimal crop side from 0.08 to 0.5. This ensured stable convergence and a more reliable evaluation in AL experiments.

ImageNet modifications ImageNet hyper-parameters were identical to TinyImageNet except for the number of epochs, which was set to 100 due to high computational cost, and the batch size, which was set to 50 to fit into a standard GPU virtual memory.

E.3.2. LINEAR EVALUATION ON SELF-SUPERVISED EMBEDDING

In these experiments, we also used the framework by [Munjal et al. \(2020\)](#). We extracted an embedding similar to App. E.2, and trained a single linear layer of size $d \times C$ where d is the feature dimensions, and C is the number of classes. To optimize this single layer, we increased the initial learning rate by a factor of 100 to 2.5, and as the training time is much shorter, we multiplied the number of epochs by 2.

E.3.3. SEMI-SUPERVISED EVALUATION

When training FlexMatch, we used the active learning framework by [Zhang et al. \(2021\)](#). All experiments contained 3 repetitions. We used the following hyper-parameters when training each experiment:

CIFAR-10. We trained WideResNet-28, for 400k iterations. We used SGD optimizer, with 0.03 learning rate, 64 batch size, 0.9 momentum, 0.0005 weight decay, 2 widen factor, 0.1 leaky slope and without dropout. The augmentations are similar to those used in FlexMatch. The weak augmentations include random crops and horizontal flips, while the strong augmentations are according to RandAugment (Cubuk et al., 2020).

CIFAR-100. We trained WideResNet-28, for 400k iterations. We used SGD optimizer, with 0.03 learning rate, 64 batch size, 0.9 momentum, 0.0001 weight decay, 8 widen factor, 0.1 leaky slope, and without dropout. The augmentations are similar to those used in FlexMatch.

TinyImageNet. We trained ResNet-50, for 1.1m iterations. We used an SGD optimizer, with a 0.03 learning rate, 32 batch size, 0.9 momentum, 0.0003 weight decay, 0.1 leaky slope, and without dropout. The augmentations are similar to those used in FlexMatch.

E.4. Ablation studies

Margin by an "oracle" network. In Section 4.3.4, we compute an "oracle" uncertainty measure. When training an oracle, we use a VGG-19 (Simonyan & Zisserman, 2014) trained on CIFAR-10, using the hyper-parameters of the original paper. We calculate the margin of each example according to this network. We note that an AL strategy based on this margin works well in the high-budget regime for both the oracle and the "student" network.

F. Additional Empirical Results

F.1. Supervised Framework

In the main paper, we presented results on 1 and 5 samples per class on average. Fig. 15 shows similar results using additional budget sizes.

In Fig. 16 we present results on additional datasets, which include ImageNet-50, ImageNet-100 and TinyImageNet. *TypiClust* outperforms all competing methods on these datasets as well.

F.2. Supervised using Self-Supervised embeddings

In Fig. 17, we show the results of a linear evaluation over self-supervised pre-trained embedding on additional datasets. We see that the initial pool selection results in a very large boost in performance - especially on ImageNet-50 and ImageNet-200.

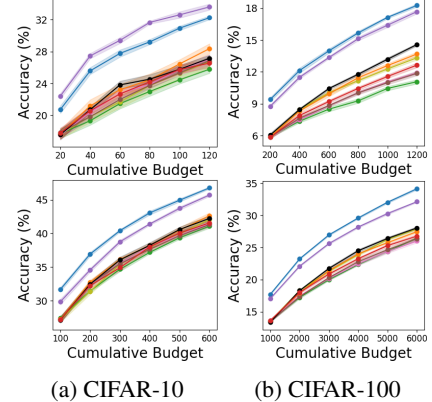


Figure 15. Additional results in the supervised framework, including an average of 2 and 5 examples per class on CIFAR10 and CIFAR100, similarly to Fig. 4.

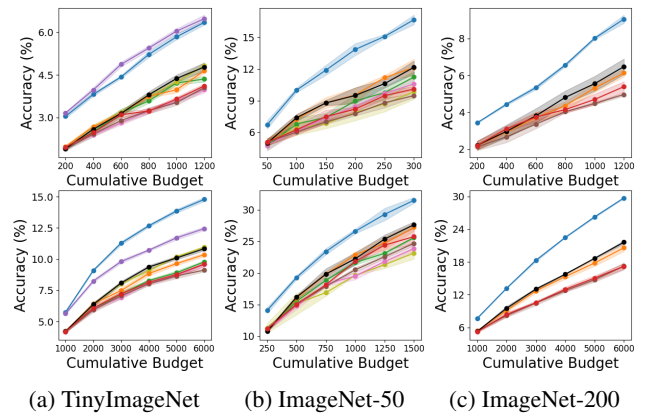


Figure 16. Similar to Fig. 4, we report the results on TinyImageNet, ImageNet-50 and ImageNet-200.

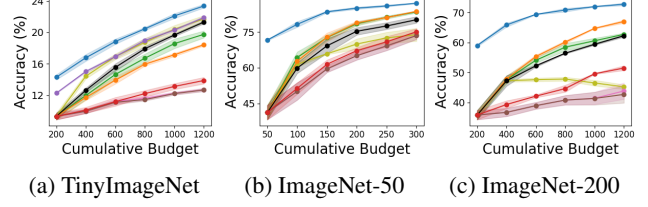


Figure 17. Similar to Fig. 5, we report the linear evaluation results on TinyImageNet, ImageNet-50 and ImageNet-200

F.3. Semi-Supervised Framework

In this section, we describe additional experiments to those plotted in Fig. 6, for the semi-supervised framework.

To test the dependency of our deep clustering variant of *TypiClust* on SCAN, we evaluated another variant based on RUC (Park et al., 2021) and denoted TPC_{RUC} . We plot its performance on CIFAR-10 and CIFAR-100 in Fig. 18. As RUC is computationally demanding, we cluster with it to the number of classes in the corresponding dataset, further sub-clustering using K-means to the desired number

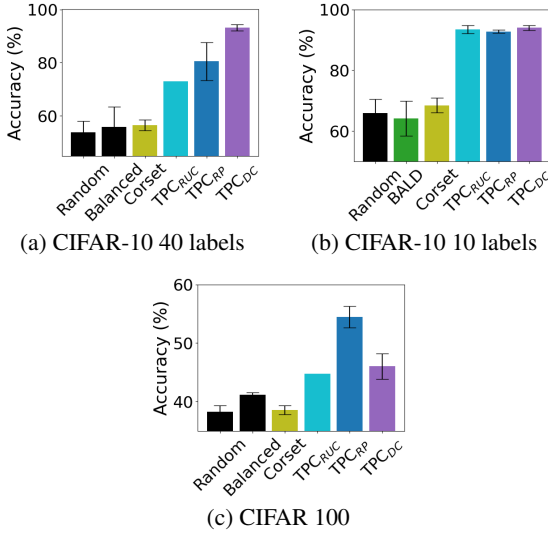


Figure 18. Similar to Fig. 6, using the TPC_{RUC} variant of *TypiClust*. (a) 40 labels on CIFAR-10, (b) 10 labels on CIFAR-10, (c) 300 labels on CIFAR-100

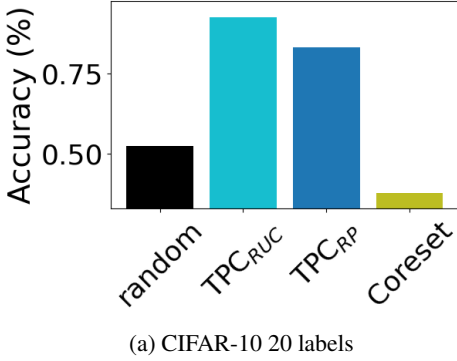


Figure 19. Similar to Fig. 6, using Semi-MMDC instead of FlexMatch. We train 20 labels on CIFAR-10, observing a large performance gain when using *TypiClust* to perform the initial selection of the labeled data.

of clusters. In all the tested settings, TPC_{RUC} surpassed the performance of the random baseline by a large margin, suggesting that using SCAN is not crucial for *TypiClust*, and may be swapped by other deep clustering algorithm.

Additionally, we performed experiments with other budgets. In Fig. 18a, we plot the same experiment as Fig. 6a, with a budget of 40 examples on CIFAR-10. We see similar results in this budget.

To see that the performance boost we see is not unique to FlexMatch, we repeat the same experiments with another competitive semi-supervised learning method, Semi-MMDC (Lerner et al., 2020). Using the code provided by Lerner et al. (2020), and following the exact training protocol, we train Semi-MMDC using 20 labels on CIFAR-10.

Similarly to the results on FlexMatch, we report a significant increase in performance when training on examples chosen by *TypiClust*. Results can be seen in Fig. 19.

We note that in all experiments we performed on the low budget regime, *TypiClust* always surpassed the random baseline by a large margin.